Evaluation of Nanoparticles for the Treatment of Chronic Neuropathic Pain

by

Chelsea Marie Harris

A thesis submitted to the Graduate Faculty of
Auburn University
in partial fulfillment of the
requirements for the Degree of
Master of Science

Auburn, Alabama
August 5, 2017

Keywords: Silica Nanoparticles, Chronic Neuropathic Pain

Approved by

Allan E. David, Chair, John W. Brown Assistant Professor, Chemical Engineering
Maria L. Auad, Associate Professor, Chemical Engineering
Bryan Beckingham, Assistant Professor, Chemical Engineering

Abstract

Pain is something that will affect every person at some point in his or her lifetime, and yet chronic severe pain remains an often-undertreated medical condition as the current treatment protocol remains largely unsuccessful in reliably and safely managing pain. Nanoparticles (NPs) have gained momentum as a promising platform for solving previously unsolved medical issues. This work aimed to investigate the usefulness of a NP platform for the selective targeting and treatment of chronic pain. By researching naturally occurring neurotransmitters in the human body that regulate the pain response in mature neurons, a NP formulation was designed. This system involved coating 120 nm silica NPs with glutamic acid through the 1-ethyl-3-(3-dimethylaminopropyl) carbodiimide (EDC) – N-hydroxysuccinimide (NHS) coupling reaction. The success of this conjugation was evaluated through a variety of analytical techniques and assays. The interactions of these particles with three main receptors in mature neurons, the γ-aminobutyric acid (GABA), α-amino-3-hydroxy-5-methyl-4-isoxazolepropionic acid (AMPA), and N-methyl-D-aspartate (NMDA) receptors, were analyzed to better understand how this particle would affect the propagation of pain signals through the nervous system. Combined with simulations of neurotransmitter effects on the hippocampal region of the brain, these results were used to develop a set of recommendations for the future progression and direction of this project.

Acknowledgements

I would like to thank Dr. Allan E. David for his support and guidance, without which this project would not have been possible. I also would like to thank the members of the David Lab for helping me with everything from proper operation of laboratory equipment to feedback on my research plans and presentations.

I would also like to thank my parents, Grey and Cindy Harris, for their continued support throughout my graduate education.

Table of Contents

List of Figures

List of Tables

Chapter 1

Introduction

Chronic pain is a widespread, yet often undertreated medical condition. Over 100 million people in the United States suffer from some form of chronic pain, totaling more than those suffering from diabetes, heart disease, and cancer combined [1]. Over three million of these suffer specifically from neuropathic pain, a condition marked by a pain state arising from "a lesion of disease of the somatosensory system"[2]. This definition is broad because neuropathic pain can be caused by a variety of diseases and conditions. This variation makes it difficult for doctors to appropriately manage a patient's pain. Further complicating the issue, neuropathic pain is often confused with nociceptive pain which describes pain caused by tissue disease or damage [3].

Over the past several decades, nanotechnology has emerged with momentum as a promising new solution to a range of previously unsolvable scientific and technological issues. Nanoparticles (NPs) offer a massive range of properties and characteristics that can be finely tuned for many applications, from electronics to medicine. More recently, exploration into their uses in the field of targeted drug delivery has gained popularity with many successes and advancements resulting [4]–[6]. Even with these successes, there has been a delay in the transfer of

nanotechnology to the field of pain management. NPs are available in sizes that are well within the range of typical synaptic gaps through which neurons communicate, and their size also lends them towards possible passage through the blood-brain barrier (BBB), a system of tight gap junctions which prevent the passage of large, ionized molecules from entering the central nervous system (CNS) [7], [8]. These size advantages, coupled with the ease of surface modifications and highly tunable characteristics, suggest that the future of pain management lies within the field of nanotechnology.

Chapter 2

Background

2.1 Challenges in Chronic Pain Management

To date, there is no standardized protocol for chronic pain management. Doctors do, however, have a typical course of treatment for pain management, starting with tricyclic antidepressants (TCAs) and topical lidocaine. If these do not work, a combination of opioid analgesics, tramadol, and calcium channel α-2-δ ligands are tested. As a last attempt at treatment, doctors will turn to anti-epileptics, N-methyl-D-aspartate (NMDA) receptor agonists, and topical capsaicin [9]. Other non-pharmaceutical options are often explored as a last attempt at pain management when pharmaceutical methods fail.

2.1.1 Pharmaceutical Methods of Pain Management

The first pharmaceutical option that doctors explore is a class of antidepressants called tricyclic antidepressants (TCAs). TCAs block the reuptake of two main neurotransmitters, serotonin and norepinephrine [10]. This inhibition in turn increases the levels of these neurotransmitters in the brain. Both serotonin and norepinephrine are involved in the inhibition of the expression of the pain state, so increasing their levels can help block the pain sensation [11], [12]. TCAs are a relatively inexpensive treatment

option, and only require one dose per day, making them an attractive option [9]. Examples of TCAs include duloxetine, venlafaxine, amitriptyline, and nortriptyline [9], [13], [14]. Generally, TCAs are tolerated well at dosages below 100 mg/day and the common side effects are not serious. These side effects can include sedation, dry mouth, constipation, blurred vision, and weight gain [9]. Once a dosage surpasses 100 mg/day, a patient's risk of sudden cardiac death may increase and the TCA levels must be monitored to ensure they are not present at levels that could cause cardiac toxicity. TCAs should be avoided entirely in patients with pre-existing ischemic heart disease or elevated sudden cardiac death risk, as well as in suicide-risk patients as overdose is a concern [9], [15].

Topical lidocaine is often used concurrently with TCAs as a localized form of pain management. Because it is applied directly to the skin, it can only relieve localized peripheral pain [16]. Topical lidocaine comes in two common forms, a 5% patch and an 8% spray. These two forms act in the same way by blocking sodium channels in the area of application [3]. Mature neurons involved in the pain response rely on sodium channels to propagate pain signals, so blocking them completely inhibits the activation of a pain sensation. The usual prescription calls for up to three patches worn simultaneously for 12 hours a day, but recently it was shown that up to four patches could be safely worn for up to 18 hours [16]. The spray has the benefit of being quickly applicable without a solid patch being worn, but it also often has a shorter period associated with relief, sometimes only four hours [17]. The patch causes mild skin irritation in some patients, but other side effects are uncommon [16]. However, due to the shortness of relief and localized treatment area, lidocaine is not a viable treatment for chronic neuropathic pain.

When this first line of defense fails, doctors will then try to manage a patient's chronic pain with opioids. Although they are not often the first choice in pain management, they are the most potent of methods, and offer the broadest range of treatable symptoms [18]. Opioids are able to treat pain through their targeting of the opioid receptors, which are three discrete types of G-coupled protein receptors called the μ-, κ-, and δ-receptors. μ-receptor ligands are the most potent and effective in managing pain symptoms. This class of opioids includes morphine, oxycodone, methadone, and tramadol. Oxycodone is unique from the others in that it also antagonizes the κ-receptor [3]. Tramadol is also unique as it works by only weakly targeting the μ-receptor. Because of this, it is not often prescribed unless several other treatment attempts have failed. While there is a large pool of options for doctors to choose from when prescribing opioids, there is no classification scheme to guide them in finding the right drug for that patient's condition or demographic [19].

Due to the prevalence and severity of long-term side effects of opioids, patients are often hesitant to use them, even if they suffer from chronic pain [20]. Even still, the prescription of strong opioids such as oxycodone and morphine for chronic pain management has quadrupled since 1980 [21]. Dosage levels and schedules can vary greatly from doctor to doctor, but typically, they fall at the upper end of the range, regardless of the patient's hesitancy [20].

This uneasiness with the potential for severe side effects is not unfounded. Nausea, constipation, and sedation are most commonly reported, but other side effects can include addiction, increased sensation to pain, and a general decrease in quality of life. Doctors are split on the topic; some argue that, when used properly, opioids pose no

risk of addiction. However, studies have shown that chronic use can lead to physiological effects, such as the strengthening of "reward pathways" in the brain, which can result in addiction [22], [23]. It is also worth noting that a significant amount of variation exists in the studies, including variations in conclusions on tolerability, commonly observed side effects, and efficacy of the drugs [24]. This uncertainty in data has prevented a standardized prescription protocol for prescription for doctors to follow from being developed. Patients with special considerations, such as the elderly or those with a higher risk of developing addiction further complicate the process of determining a universal prescription protocol [22], [25].

When opioids singularly do not work to alleviate chronic pain, some doctors will choose to try them in combination with TCAs. Sometimes this pairing will result in a heightened response; however it also increases the patient's probability of suffering from undesirable side effects from both medications [26], [27].

Next in the line of options are anticonvulsant medications. These compounds, which include gabapentin and pregabalin, work by binding to the α-2-δ subunit of voltage-gated calcium channels [9]. Several types of neurons possess these receptor channels, which are involved in the propagation of signals through a neural network. An influx of calcium will depolarize a cell, and at a certain threshold result in the formation of an action potential [28]. Medications that interact with these receptors will therefore have an effect on signal propagation. However, the neuronal targets of anticonvulsants are not necessarily involved in the pain response, so efficacy can be limited. Studies have yet to reach a conclusion on the effectiveness of anticonvulsants for pain management. Some research has supported the hypothesis that anticonvulsants are useful in pain

alleviation while other studies have shown no improvement in the pain condition whatsoever [19]. Dosing issues add to the probability that treatment will fail, since dosage level must be tailored to each patient by starting at the low end of the range and titrating to an effective dose [9], [29]. Reported side effects include dizziness, somnolence, peripheral edema, and cognitive and gait impairment. Special considerations must still be taken for elderly patients [9]. These details collectively reduce the likelihood that a patient will comply with an anticonvulsant-based treatment plan.

Because anticonvulsants were not intentionally designed for pain treatment, they are often combined with other forms of treatment if they fail when used alone. In one study, gabapentin and morphine were administered together and resulted in increased pain relief than either drug taken alone. Although some side effects were observed, they were nothing out of the ordinary for either medication [20]. Gabapentin has also been studied with oxycodone and an increase in pain relief in diabetic neuropathy was demonstrated over gabapentin alone [30]. TCAs are also commonly paired with gabapentin, such as one study where nortriptyline was administered in tandem and a significant reduction in neuropathic pain was observed over the individual drugs. A large percentage of the study population experienced a decrease in pain intensity and an increase in pain relief, with dry mouth being the only common side effect [13]. Another common anticonvulsant, pregabalin, was taken while patients also wore 5% lidocaine patches. This combination was effective in pain management and the treatment was well tolerated in patients with post-herpetic neuralgia and diabetic polyneuropathy [31].

When all of the previously mentioned medications fail to sufficiently manage a patient’s chronic pain, doctors will try non-traditional medications. These include a wide

variety of medications developed for other conditions, such as selective serotonin reuptake inhibitors (SSRIs), N-methyl-D-aspartate (NMDA) receptor agonists, and topical capsaicin. SSRIs are a form of antidepressants which block serotonin uptake and include buproprio, citalopram, and paroxetine, while NMDA receptor agonists include medications such as dextromethorphan and memantine [19], [32]. NMDA receptor agonists block the activation of the NMDA receptor, which is thought to play a role in the health of neurons [19], [33]. Regardless, NMDA receptors rarely result in anything more than limited improvement to the pain condition. Capsaicin is similar to topical lidocaine in that is it a localized treatment applied to the skin, but studies of the effectiveness of capsaicin for neuropathic pain are varied in conclusion. Additionally, patients often suffer from a burning sensation in the area of application, which only adds to the pain being experienced [19], [34]. Mexiletine, an antiarrhythmic lidocaine analog, is used infrequently and often shows limited benefits over a placebo. However, this drug is seldom used because side effects can become serious at higher dosages and are sometimes not worth the risk for a modest relief in the pain condition [19], [32].

Non-steroidal anti-inflammatory drugs (NSAIDs) are another option in pain management; however, they are typically not strong enough to mask the severity of neuropathic pain. Many of the most common NSAIDs work through the inhibition of the synthesis of prostaglandins by blocking the production of the enzyme cyclooxygenase (COX) [35]. There are two forms of COX: COX-I and COX-II. It has been theorized that COX-I may play a limited role in some types of pain expression, but COX-II is a main player in the body's response to pain and inflammation. Because of this, many typical NSAIDs inhibit the production of COX-II. Examples of such include aspirin and

diclofenac. NSAIDs are a popular treatment for lower threshold pain conditions, and one third of NSAIDs prescribed for use against acute or chronic pain in 2000 were COX-II inhibitors [21], [35]. However, NSAIDs can cause a variety of side effects if used for an extended period of time which include ulceration, bleeding, and GI perforation [35]. Because they work through mechanisms entirely separate from opioids, they are sometimes tried in combination. Pairing tramadol with acetaminophen resulted in a reduction in pain intensity and sleep interference, and an increase in quality of life and mood when compared to each of the drugs taken alone. Nausea was the only commonly observed side effect [36].

2.1.2 Non-pharmaceutical Methods of Pain Management

Both patients and doctors will often explore routes of treatment that do not involve medication, especially when they have tried and failed with medications previously. These methods include physical exercise, massage therapy, yoga and meditation, acupuncture, transcutaneous electrical nerve stimulation (TENS), and cognitive behavioral therapy (CBT). While patient interest in these types of treatments is growing, the uses of physiotherapy and psychotherapy for pain management are declining, and only 4% of visits with a physician for pain management result in the prescription of one of the above [21]. However, the number of studies focusing on the benefits of these methods is increasing, so it may be that their efficacy is not yet understood [20].

2.2 Properties and Characteristics of Silica Nanoparticles

Due to the wide applicability of nanotechnology in the search for answers to many scientific and technological questions, understanding of the potential applications of nanoparticles has greatly increased over the past few decades. A nanoparticle is defined as any particle whose size falls in the range of 1 to 100 nanometers (nm) [8]. They are available in many different types of materials, including gold, iron oxide, and silica, and each come with their own unique set of advantages and disadvantages.

Silica NPs are generally considered non-toxic and safe for *in vivo* use; however unmodified amorphous silica has reportedly caused inflammation and liver damage [37]–[39]. Therefore, potential toxicity must be considered when silica NPs are chosen as a platform for use in humans internally. This size range offers a platform for small molecule delivery which can easily disperse throughout the body and escape rapid renal clearance as well as pass through the blood-brain barrier (BBB). While the ability to pass the BBB raises some toxicity concerns, this also makes them an attractive option for CNS drug delivery applications [7]. Many medications have the potential to be useful in the treatment of neurological diseases but are unable to pass the BBB making them a non-viable treatment option. In addition to clearing the BBB, small NPs are also able to be uptaken by cells, opening the door for intracellular drug delivery applications [5].

Due to the fact that there are numerous materials that NPs can be synthesized from, there are, by extension, many surface modifications possible. Polymers, such as polyethylene glycol (PEG) and other hydrophilic polymers, are common choices for surface attachments as they increase circulation time in the body and shield the NPs from being recognized as a foreign body by the immune system. Polymers can also encourage

accumulation of NPs at certain tumor sites, an application useful in cancer drug delivery as it not only illuminates the presence and exact location of a tumor but also allows for the direct calculation of tumor size [4]. Biologically active molecules may easily be attached to the surface of NPs through a polymeric crosslinker or directly to the particle itself which can increase cellular uptake and retention time in the body [5], [6].

Chapter 3

Experimental Details

The majority of the work in this thesis falls into two main categories: nanoparticle formulation and *in vitro* assessments of particle effects. In the following sections, the diagnostic methods and tools used in evaluating these two aims are described.

3.1 pH Measurement

An Orion Star A211 pH Benchtop Meter from ThermoScientific was used to determine the pH of various solutions throughout NP formulation reactions. A pH meter determines the activity of hydrogen ions in a given solution by measuring the difference in electrical potential between the pH electrode, which is inserted into the solution of interest, and a reference electrode. The Orion Star uses a gel-filled combination electrode, which combines a glass bulb for detecting solution pH, and a reference half-cell filled with gel. The glass electrode can detect hydrogen ions through the presence of a positive charge that causes a potential difference on the surface of the electrode that is measured as a voltage reading. This reading is sent to the meter and compared with the constant voltage reading of the reference electrode [40]. This potential difference can be modeled using the Nernst equation:

$$E = E_o - \frac{RT}{nF}\ln(Q) \tag{3.1}$$

where E is the potential difference, E_o is the standard reduction potential, R is the ideal gas constant, T is the temperature of the solution, n is the number of electrons exchanged in the reaction, F is Faraday's constant, and Q is the reaction quotient for the reaction. The reaction quotient, Q, is equivalent to the difference of the pH outside the electrode and inside the electrode. Because the inside of the electrode has a constant pH, this substitution allows the calculation of the solution pH, and assuming the measurement is performed at room temperature:

$$E = E_o + 0.0591 \log \frac{[H^+_{inside}]}{[H^+_{outside}]} \tag{3.2}$$

Once the concentration of ions outside of the cell is calculated from Equation 3.2, the pH of the solution is calculated using Equation 3.3 [41]:

$$pH = -\log([H^+_{outside}]) \tag{3.3}$$

This equation directly relates the presence of hydrogen ions detected by the glass electrode to the pH of the solution, giving an accurate measurement to ±0.002 pH units. This technique was used to ensure that the reactions used in the conjugation of both GABA and glutamic acid to the surface of aminated silica nanoparticles were completed at the desired pH.

3.2 Spectrophotometry and Spectroscopy

A FlexStation 3 and a SpectraMax i3 by Molecular Devices were used in this work. Spectrophotometry is used for the measurement of how much a molecule, chemical, or solution absorbs or transmits light at a certain wavelength. Measurements made between 185 – 400 nm are possible with a spectrophotometer that can detect wavelengths in the ultraviolet and visible (UV-Vis) light ranges. Absorbance

measurements are colorimetric, with the chemical of interest absorbing the complimentary color to its visible color. Spectrophotometers work by sending light from a light source through a monochromator and then into the solution of interest. Light will pass through depending on the properties of the solution, and then a digital readout of the light detected on the other side of the sample is given. This fraction of light that passes through is known as the transmittance, which is calculated using Equation 3.5:

$$T = \frac{I_t}{I_o} \tag{3.4}$$

Where I_t is the light intensity of the transmitted light and I_o is the intensity of the light sent to the solution. Transmittance can then be used to calculate absorbance which is related through Equation 3.6 [42]:

$$A = -\log(T) \tag{3.5}$$

Spectrophotometers typically have the option to output data either in transmittance or in absorbance, whichever is more useful to the researcher. In this work, several color-based assays were performed in order to measure concentrations of thiol groups, polyethylene glycol (PEG) molecules, and chloride ions in solution. This assays used spectrophotometry to detect absorbance of these molecules of interest at certain characteristics wavelengths.

Spectrophotometers also have the capability to perform spectroscopy, which is useful in the case of measuring fluorescence from a sample. Like in spectrophotometry, light is sent through a monochromator to a sample at a certain wavelength to excite the sample causing it to emit light. The fluorescence is measured at a 90° angle from the incident light to avoid interference from any light that may be transmitted through the sample. The machine then returns the level of emitted light as a measure of the strength

of the fluorescent behavior by the sample [43]. Several fluorescence-based assays were used to detect concentrations of potassium ions, calcium ions, and fluorescamine in various solutions.

3.3 Fourier Transform Infrared Spectroscopy

Fourier Transform Infrared (FTIR) Spectroscopy is a specialized type of spectrophotometry that measures the amount of absorption by certain material over the infrared spectrum. A Fourier transform is necessary to convert the raw data, called an interferogram, collected by the machine into a spectral graph. This spectrum allows the presence of certain molecules to be elucidated by the presence of a characteristic peak in the spectrum.

The FTIR spectrometer sends a beam of infrared light through a beamsplitter which splits the light into two beams that are 90° apart. One beam travels to a fixed mirror and is returned to the beamsplitter, whereas the other travels to a moving mirror which moves over a certain distance. The beam then travels back over the total path length from the moving mirror to the beamsplitter and recombines with the other light beam. The path length difference between the two beams creates the interferogram due to constructive and destructive interference of the two beams. This recombined beam is sent to the sample, the sample absorbs any wavelength that is associated with the molecules present, and the differences in energy at each point in time detected by the machine at different wavelengths are recorded. A Fourier transform, defined generally in Equation 3.4, is performed on the data to convert the intensity over time data to intensity over frequency.

$$F(\omega) = \int_{-\infty}^{+\infty} f(x) e^{i\omega x} dx \quad (3.6)$$

where F(ω) is the frequency domain or spectrum for a given ω angular frequency, f(x) is the time domain function called the interferogram for a given x where x is total path length difference, and i is the square root of -1 [44]. The spectra collected can be analyzed for characteristic peaks and their relative intensities can be used to determine relative compositions of components in the sample. A Nicolet IR100 FT-IR Spectrometer from Thermo Scientific was used to determine if glutamic acid had successfully been attached to the surface of aminated silica NPs by comparing the coated NP spectra to that of free glutamic acid and unaltered Si NPs.

3.4 Dynamic Light Scattering

Dynamic light scattering (DLS) was performed on batches of Si NPs to measure particle size and the relative distributions of those sizes using a Malvern ZetaSizer. A laser beam is sent through a small sample of about 1 ml in a plastic cuvette. Due to the natural movement of particles in solution, called Brownian motion, the light is scattered at varying intensities and this change in scattering is measured over time; this in turn is related to the size of the particles interfering and can give a measurement of such. The relationship between particle size and this motion can be determined using the Stokes-Einstein equation defined in Equation 3.7:

$$D = \frac{RT}{6N_A \pi \eta a} \quad (3.7)$$

This equation relates D, the diffusion coefficient for a sphere, with radius, a, to the dynamic viscosity, η, for a particle experiencing Brownian Motion, where N_A is Avogadro's Number, R is the ideal gas constant, and T is the temperature of the solution

[45]. Properties of the particle material and dispersant must be provided to the software so that the particle size can be accurately calculated.

3.5 Zeta Potential

Another method for characterizing NPs is measuring their zeta potential in a given solvent. Zeta potential (ζ) describes the magnitude of the charge that exists at the interface of particles in the solution. Particles with a high ζ, typically greater than ±30 mv, are stable in solution, whereas particles with a low ζ are not. Particles with extremely low ζ will aggregate rapidly making them unreliable for experimentation. Zeta potentials below ±5 mV are considered very unstable and potentials above ±61 mV are highly stable. This measurement ensures an appropriate solvent is chosen for optimal particle stability over time for both storage and experimentation [46]. A Malvern Zetasizer Nano-ZS was used for zeta potential measurements.

3.6 Polyethylene Glycol Assay

This assay is performed when the concentration of free polyethylene glycol (PEG) in a solution is desired. Solutions of 2% barium chloride and 0.002 N iodine are both added in 2:1 ratios with the unknown solution. Upon mixing, the barium chloride dissociates and forms barium iodide which in turn forms a complex with free PEG [47]. This complex forms a robust color and absorbance can be measured at 535 nm alongside a range of PEG-barium iodide solutions of known concentrations to determine free PEG concentration.

3.7 Fluorescamine Assay

Fluorescamine assay was used in several applications to detect primary amines in solution. In this protocol, a 1 mg/ml solution of fluorescamine in dimethyl sulfoxide (DMSO) is added to a solution with an unknown concentration of primary amines in a ratio of 1:4. The mixture is allowed to react for 10 minutes (min) protected from light. During this reaction time, the non-fluorescent fluorescamine reacts with primary amines to form a fluorophore which can be excited at 392 nm with an emission given at 478 nm. Hydrolysis products are also formed but do not fluoresce so they do not interfere with results. This reaction gives highest yields at pHs above 7 as amine groups are more likely to be reactive due to deprotonation above this level [48]. A standard curve can be developed for comparison of unknowns using ethanolamine in water. Literature suggests this assay may be useful in the range of 0 to 1 mg/ml primary amines.

3.8 Thiol Assay

Measurement of thiol groups present in a solution was done using 5,5'-dithio-bis-[2-nitrobenzoic acid] (DTNB), commonly known as Ellman's Reagent. This molecule reacts with thiol groups to produce a chromophore whose absorbance can be measured at 412 nm using a spectrophotometer. A standard curve in the range of 0 to 1.5 mM thiols can be prepared using cysteine hydrochloride monohydrate in PBS. This produces a linear standard curve which is very reliable and robust.

3.9 Potassium Assay

Potassium channel activity was analyzed using the FLIPR Potassium Assay Kit from Molecular Devices. This kit takes advantage of the conversion of a fluorescent dye which binds to thallium ions that have been transported into cells either through voltage-gated or ligand-gated potassium (K^+) channels. Therefore, fluorescent readout is an indicator of the amount of K^+ channels open at a given time since thallium ions will have entered the cell only through these open channels. In the version of this kit used here, the dye contains an acetoxymethyl (AM) ester which amplifies permeability to adherent cells through passive diffusion. Upon entering the cell, the AM ester is cleaved and the molecule is available for binding to free thallium ions. The bound dye can be excited at 485 nm with emission collected at 525 nm [49].

3.10 Chloride Assay

Similar to the potassium assay, BioVision's Chloride Colorimetric Assay Kit was used to monitor chloride activity in cells. This assay employs 2,4,6-tripyridyl-s-triazine's (TPTZ) reactivity with mercury (Hg^{2+}) and iron (Fe^{2+}) ions. TPTZ prefers to bind with Hg^{2+}, however if chloride ions are present, Hg^{2+} will prefer forming $HgCl_2$ over the TPTZ complex. This uses up the Hg^{2+} ions forcing the TPTZ to bind with the Fe^{2+} ions instead. This TPTZ-Fe^{2+} complex absorbs very strongly at 620 nm. If no chloride is present to bind with the Hg^{2+} ions and the TPTZ-Hg^{2+} complex forms, it is colorless at 620 nm so no significant absorbance will be detected [50]. This measurement can be used to indirectly determine the amount of chloride present in the solution.

3.11 Calcium Assay

Enzo Life Science's FluoForte Calcium Assay Kit was used to study calcium mobilization in various cell types. The FluoForte dye is activated by intracellular calcium ions so that calcium mobilization may be monitored. Upon activation, the dye will fluoresce with an excitation wavelength of 530 nm and emission at 570 nm using a spectrophotometer. The assay works well with both adherent and non-adherent cell lines, and offers high sensitivity to low levels of intracellular calcium [51].

3.12 Mammalian Cell Culture

Two cell lines were cultured and maintained throughout these experiments. SH-SY5Y cell line was created from a human neuroblast from neural tissue. These cells are both adherent and suspension cultures. They were cultured in a medium composed of 15% fetal bovine serum (FBS), 1% antibiotics, and the remainder an equal mixture of Ham's F12 and Eagle's Minimum Essential Medium (EMEM). These cells are typically used in neurotransmitter-related studies as they express the GABA, AMPA, and NMDA receptors.

The second cell line used was the Chinese hamster ovary (CHO-K1) cell line sourced from the ovary of the Chinese hamster. These cells are adherent and were grown in a medium of 10% FBS, 1% antibiotics, and the remainder Ham's F12. CHO cells do not express any of the neuronal receptors that the SH-SY5Y cells contain. Both cell lines were stored at 5% CO_2 and 37°C.

3.13 Modeling of Neural Circuits using NEURON Software

A circuit of 100 neurons of various phenotypes common to the hippocampus was modeled using the NEURON software package originally developed by Michael Hines, John W. Moore, and Ted Carnevale at Yale and Duke Universities [52]. This software allows the behavior and structure of both individual neurons and networks of neurons to be simulated using a variety of models. Here, a network of 100 neurons with varying properties was modeled using the Hodgkin-Huxley model. This mathematical model describes cellular behavior in terms of electrical circuits in order to study action potential initiation and propagation at the cellular and network levels. The cell membrane, which biologically is comprised of a lipid bilayer, is given both a resting potential, V_m, a resistance, R_m, and a capacitance, C_m. These variables describe how the cell membrane behaves when a potential difference exists between the intracellular fluid and extracellular medium. The most basic neuronal cell type will contain only leak channels, which allow for passive diffusion of ions, such as sodium and potassium, across the membrane. This passive behavior is responsible for the maintenance of the cell's resting potential. However, neurons are not typically dominated by passive properties. There are many different channel types that a neuron's membrane may contain; the most common of these are the sodium (Na^+), potassium (K^+), and calcium (Ca^{2+}) channels. These channels in reality may be voltage or ligand-gated depending on the cell type, but the Hodgkin-Huxley model describes all channels using electrophysiological concepts. These individual channel types are modeled in the circuit as a resistor, R_{ion}, which describes how resistant the channel is to ion flow, a current, I_{ion}, which is dependent upon the amount, type, and direction of flow of ions passing through that channel, and a battery,

E_{ion}, which indicates direction of ion flow by comparing the individual potential associated with that ion relative to the entire cells' membrane potential. These electrical components simulate a physiological response upon the receiving of a chemical signal. When sodium channels are activated due to this incoming stimulus, Na^+ ions are allowed to rush into the cell, depolarizing it from its resting potential. This depolarization will trigger the opening of other channels such as the potassium channels, allowing K^+ ions to rush out of the cell. This serves to balance out the large positive gain in charge inside the cell caused by the sodium ion influx, thus returning the cell to its resting state. The majority of neurons are, however, not this simple and contain many different receptor channels with varying behaviors and effects on cell potential. A single neuron containing the three channel types mentioned above can be modeled as a circuit shown in Figure 1 [53].

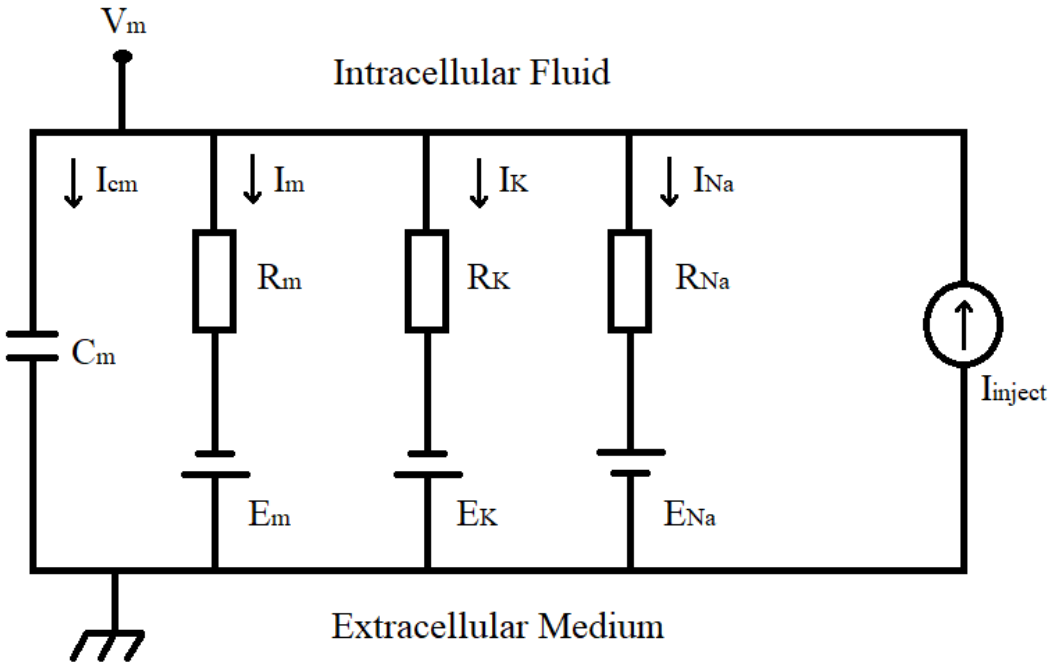

Figure 1. Hodgkin-Huxley model of a neuron with passive and ion channels.

This model may be altered to incorporate more channel types by adding the corresponding resistors, batteries, and currents. Using this model, a neuron's behavior over time with varying voltage potentials may be modeled using Equation 3.7:

$$C\frac{dV}{dt} = -\sum I_{ion} + I_{inject} \tag{3.7}$$

where C is capacitance, $\frac{\mathrm{dV}}{\mathrm{dt}}$ is the derivative of voltage across the membrane with respect to time, $\sum \mathrm{I_{ion}}$ is the cumulative charge due to each ion channel present, and $\mathrm{I_{inject}}$ describes the current injection input to the model by the user as a stimulus. The system may be further described by defining current behavior, as shown in Equation 3.8 [53]:

$$I_{ion} = G_{ion}(V - E_{ion}) \tag{3.8}$$

Where G_{ion} is the maximal conductance of that ion, V is the voltage of the system, and E_{ion} is the Nernst potential of that ion. The maximal conductance of an ion is based on the maximal conductance for the specific ion over a given area as well as the number of activation and inactivation gates for a given ion channel type [53].

These mathematical models are implemented by developing individual files in the NMODL language for each unique cellular unit, including each type of channel. The NEURON language may be interfaced with Python 2.7 to build individual neurons with the desired components and properties. NEURON allows these individual cells to be connected through user-defined synaptic junctions so that a neural network may be simulated.

In this work, a network of 100 neurons was developed to study the effect of γ-aminobutyric acid (GABA) on the hippocampus. The hippocampus is thought to play a large role in learning and plasticity over time, including mediating the long-term response to chronic pain [54]. The hippocampus is primarily comprised of two types of neurons:

pyramidal neurons and interneurons. A typical hippocampus is 90% pyramidal neurons and 10% interneurons [55]. This was used to build a model of 90 pyramidal neurons, divided into three subclasses with varying properties, and 10 interneurons. Because the signal propagation by interneurons is largely dominated by their dendrite length, the interneurons were modeled using a two-compartment scheme with a soma, or cell body, and dendrite. The pyramidal neurons were modeled using a singular soma. While this is not biologically accurate, the cellular components used here are largely responsible for signal reception and propagation, making the model applicable. Table 1 shows the physical characteristics and properties, including diameter (D) in µm, length (L) in µm, resistance (R_a) in Ω*cm, and capacitance (C_m) in µF/cm^2 , used to model the somas and dendrites of the respective cell types.

Table 1. Physical characteristics and properties of pyramidal neuron subclasses and interneurons.

	Soma				**Dendrite**			
Cell	D (µm)	L (µm)	R_a (Ω*cm)	C_m (µF/cm^2)	D (µm)	L (µm)	R_a (Ω*cm)	C_m (µF/cm^2)
Pyramidal A	24.75	25	200	2.5	-	-	-	-
Pyramidal B	24.75	25	200	2.5	-	-	-	-
Pyramidal C	24.75	25	200	2.5	-	-	-	-
Interneuron	15	15	3375	1	10	150	150	1

These values were used to create individual cell classes in NMODL that were used to create a neural network. The cell types also contained a variety of ion channels, whose various potentials, conductances, and associated time constants must be defined. As previously discussed, each channel present has an associated voltage potential, E_{ion}; these values are given for four channel types, leak, calcium (Ca), sodium (Na), and potassium (K), in Table 2.

Table 2. Potential values for various ion channels in pyramidal neuron subclasses and interneurons.

Cell	E_{Leak} (mV)	E_{Ca} (mV)	E_{Na} (mV)	E_{K} (mV)
Pyramidal A	-72	120	45	-80
Pyramidal B	-72	120	45	-80
Pyramidal C	-72	120	45	-80
Interneuron – Soma	-70	-	45	-80
Interneuron – Dendrite	-70	-	45	-80

Additionally, the conductances associated with each ion channel type must be defined. The value of G_{ion} in Equation 3.8 is calculated using the $\bar{g}_{ion}$ values given in Table 3. Here, $\bar{g}_{ion}$ is the conductance of that ion over a certain unit area. This unit area is the surface area of the cell, which is based on the diameter and length parameters shown in Table 2. Table 3 shows the specific conductances for passive leak channels (leak), high voltage-activated calcium channels (Ca), sodium channels (Na), persistent sodium channels (Nap), delayed rectifier potassium channels (Kdr), slow after-hyperpolarization calcium channels (sAHP), voltage-gated persistent muscarinic channels (im), and persistent potassium channels (Kap). Additionally, Table 3 defines the time constant associated with calcium pooling, $\tau_{Ca\ pool}$, which describes how long calcium is allowed to accumulate within the cell before a reaction is initated.

Table 3. Conductances and time constants for various ion channels in pyramidal neuron subclasses and interneurons

	Pyramidal A	**Pyramidal B**	**Pyramidal C**	**Interneuron (Soma)**	**Interneuron (Dendrite)**
$\bar{g}_{leak}$ **(S/cm^2)**	5.5×10^{-5}	5.5×10^{-5}	5.5×10^{-5}	5.0×10^{-5}	5.0×10^{-5}
$\bar{g}_{Ca}$ **(S/cm^2)**	5.5×10^{-5}	5.5×10^{-5}	5.5×10^{-5}	-	-
$\bar{g}_{Na}$ **(S/cm^2)**	3.0×10^{-2}	2.7×10^{-2}	3.0×10^{-2}	3.5×10^{-2}	1.0×10^{-2}
$\bar{g}_{Nap}$ **(S/cm^2)**	1.42×10^{-4}	1.42×10^{-4}	1.42×10^{-4}	-	-
$\bar{g}_{Kdr}$ **(S/cm^2)**	3.5×10^{-3}	2.0×10^{-3}	3.5×10^{-3}	8.0×10^{-3}	3.0×10^{-3}
$\bar{g}_{sAHP}$ **(S/cm^2)**	3.0×10^{-4}	1.5×10^{-4}	1.15×10^{-4}	-	-
$\bar{g}_{im}$ **(S/cm^2)**	6.0×10^{-4}	6.0×10^{-4}	6.0×10^{-4}	-	-
$\bar{g}_{Kap}$ **(S/cm^2)**	2.0×10^{-3}	2.0×10^{-3}	2.0×10^{-3}	-	-
$\tau_{Ca\ pool}$ **(ms)**	1000	1000	1000	-	-

The differences in these channel values dictates the variability in behavior of the pyramidal neuron subclasses and the difference in pyramidal neurons versus interneurons [55]–[58].

Chapter 4

Results and Discussion

4.1 Analysis of γ-aminobutyric Acid-Coated Silica Nanoparticles

γ-aminobutyric acid (GABA) is used as one of the body's main neurotransmitters for the inhibitory pain response in mature adults. GABA works by targeting the $GABA_A$ and $GABA_B$ receptors which are responsible for fast and slow inhibition of signal propagation, respectively. These two receptor classes are entirely separate in structure; $GABA_A$ receptors are ligand-gated chloride channels and $GABA_B$ receptors are G-coupled protein receptors [59]–[61]. This difference in structure is responsible for their varying responses to stimuli. Figure 2 shows the molecular structure of GABA.

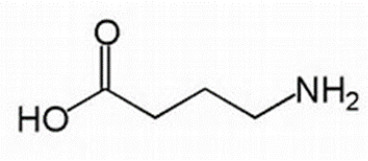

Figure 2. Molecular structure of GABA.

To take advantage of this behavior, GABA was attached to the surface of 120 nm aminated silica nanoparticles (NPs) from nanoComposix. GABA was dissolved into PBS at a concentration of 1.1 mM and combined with 2 mM ethylenediaminetetraacetic acid (EDTA). The pH of this solution was raised to 8 using NaOH to bring the solution into

the optimal range for the conjugation reaction. Traut's reagent (2-iminothiolane hydrochloride) was added to the solution to a concentration of 2.7 mM. Traut's reagent reacts with primary amines in solution to form a bond with a free thiol group. This solution was incubated for 1 hour at room temperature with agitation to complete the binding of GABA to Traut's reagent which involves the interaction of the GABA amine and the Traut's molecule.

4.1.1 Measurement of Thiol Concentration

A set of standards was created by dissolving cysteine hydrochloride monohydrate in PBS from 0 to 1.5mM. 125μL of each standard and the GABA/Traut's molecule was combined with 25 μL of Ellman's reagent (5,5'-dithiobis-(2-nitrobenzoic acid)) and 1250 μL of PBS. This solution was agitated for 15 min at room temperature. 200 μL of each solution was then added in triplicate to a clear 96 well plate and absorbance was measured at 412 nm. The standard curve generated is seen below in Figure 3.

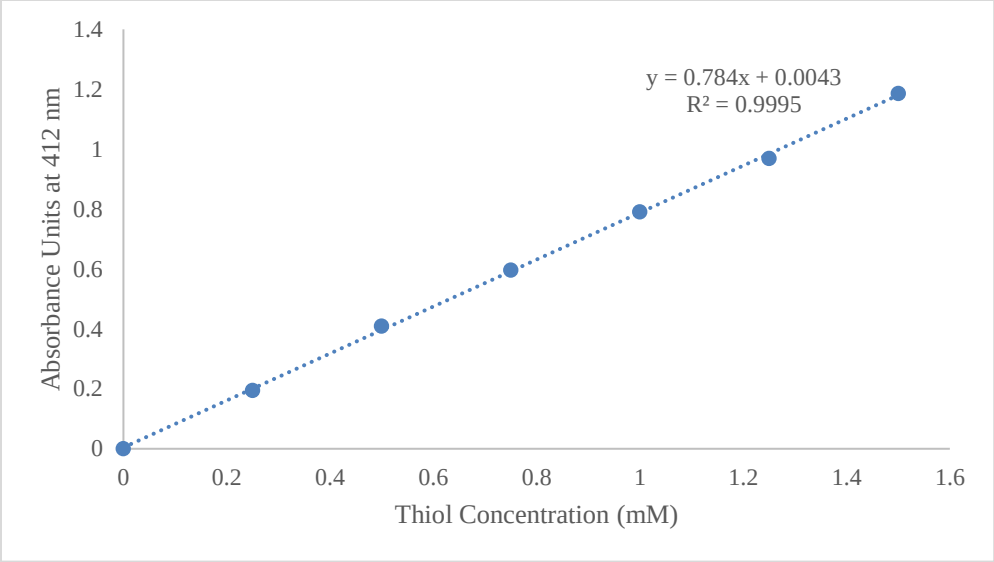

Figure 3. Cysteine standard curve for thiol assay.

This standard curve was very reproducible. The assay determined that for the first two batches of thiolated GABA, 36.4±0.1% and 26.8±0.3% of the GABA available was thiolated. However, the stock of Traut's reagent had absorbed water, so these results were not trustworthy. Repeating this reaction using new Traut's reagent resulted in a lower yields with batches in the 8-10% range of thiolation. Figure 4 shows the percent of thiolation over 72 hours for three batches of GABA.

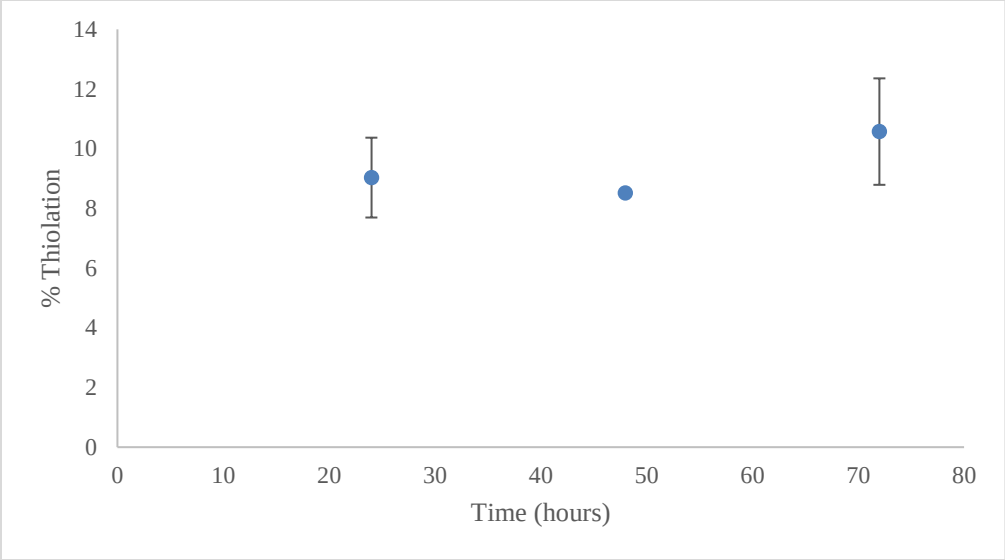

Figure 4. Percent thiolation of GABA over 72 hours.

This study confirmed that a reaction time of just 24 hours was acceptable for maximum thiolation and that approximately 9% thiolation could be expected for each reaction.

4.1.2 PEGylation of Aminated Silica Nanoparticles

The next step in the goal of attaching GABA to the surface of Si NPs is the PEGylation of the particles. 2000 MW polyethylene glycol (PEG) with a maleimide (Mal) group on one end and an N-hydroxysuccinimide (NHS) group on the other (Mal-PEG-NHS) was attached to the aminated Si NPs by combining the Mal-PEG-NHS with 120 nm Si NPs in 4-(2-hydroxyethyl)-1-piperazineethanesulfonic acid) (HEPES) and $1x10^{-5}$ mol of 1-ethyl-3-(3-dimethylaminopropyl) carbodiimide (EDC) at pH 8. This solution was allowed to react overnight with agitation. The particles were then washed using three cycles of centrifugation at 14800 RPM for 10 min followed by supernatant removal, resuspension in H_2O, and sonication. The supernatants from each wash were saved for later testing as an indirect measurement of successful attachment.

4.1.3 Determination of PEG Attachment

The amount of Mal-PEG-NHS collected in the three NP washes was used as a method to determine indirectly how much Mal-PEG-NHS had been successfully attached. A standard curve was developed using Mal-PEG-NHS in water at concentrations from 0 to 0.250 mg/ml. 50 µL of each standard or the washes was combined with 100 µL of 2% BaCl and 100 µL of 0.002 N iodine in a 96 well plate in triplicate. These were allowed to react at room temperature for 8 min and then the samples were shaken at a low intensity for 120 s and the absorbance at 535 nm was determined. Figure 5 shows a typical standard curve generated for this assay.

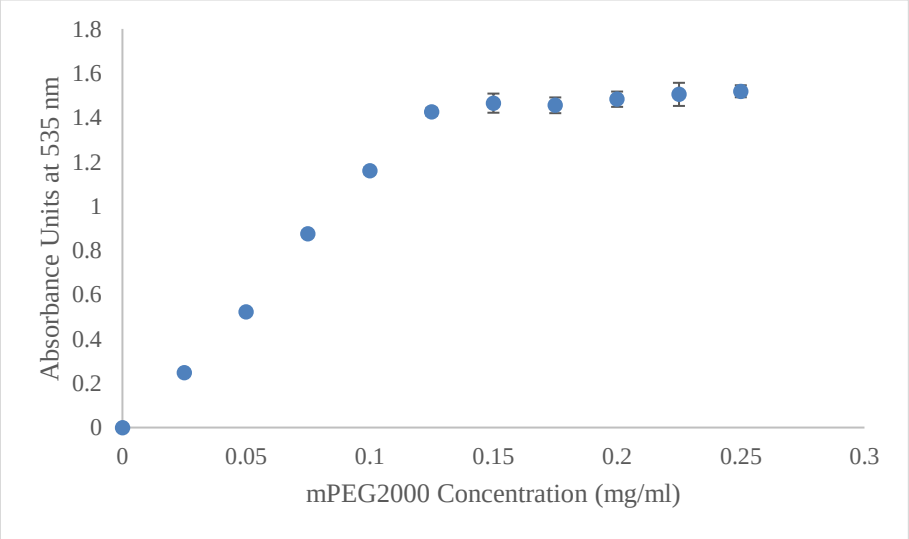

Figure 5. Standard curve for determination of PEG in NP washes.

Using this curve, it was found that Wash 1 contained 10.5 mg/ml Mal-PEG-NHS, Wash 2 contained 0.45 mg/ml, and Wash 3 contained 0.0085 mg/ml, giving a total of 10.9 mg PEG not attached to the Si NPs. An initial quantity of 10 mg of PEG was added to the

solution, which indicates that there was no attachment of Mal-PEG-NHS to the NP surface and that the assay may be overestimating the amount of Mal-PEG-NHS present. Upon further consideration, this nanoparticle formulation was abandoned, due to the non-selective nature of the resulting surface arrangement. The GABA molecule consists of only a four carbon chain with an amine at one end and a carboxyl group at the other, so there is not much freedom for attachment configurations. The thiolation of GABA replaced the primary amine with a thiol, leaving only the carboxyl group free on the surface of the nanoparticle. A nanoparticle whose surface is covered with carboxyl groups would not be biologically active or relevant so the formulation was abandoned.

4.2 Analysis of Glutamic Acid-coated Nanoparticles

The GABA receptor class remained a target of interest, so a molecule that resembled GABA but also had a third functional group that would allow for binding was investigated. Glutamic acid, whose structure is shown in Figure 6, is a five chain carbon molecule with a carboxyl group on either end and an amine group on the second carbon.

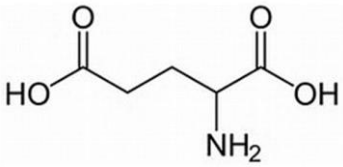

Figure 6. Molecular structure of glutamic acid.

This arrangement allows for the conjugation of the carboxyl group on the first carbon, leaving the remainder of the molecule with the same structure as the four carbon GABA. Glutamic acid is not only structurally an attractive choice, but also biologically. When it

deprotonates it becomes glutamate, a main neurotransmitter involved in the activation of neurons [62].

4.2.1 Conjugation of Glutamic Acid to Aminated Silica Nanoparticles

The EDC/NHS coupling reaction was again employed in this conjugation. The carboxyl group on the primary carbon was the desired target for binding to the NPs, however there was another carboxyl group on the fifth carbon. To push the reaction towards binding with the first carboxyl group, the pH of the solution was adjusted to 3. The pKa value of the first carboxyl group on glutamic acid is 2.10, that of the amine is 4.07, and the last carboxyl group is 9.47. Adjusting the pH to 3 would ideally cause the first carboxyl group to become deprotonated while the other two functional groups remained neutral. A ratio of 1:10:25 was used to determine amounts of glutamic acid to EDC to NHS used for the reaction. A $6.8x10^{-2}$ M solution of glutamic acid in PBS was made and the pH was adjusted to 3 using HCl. EDC-HCl and NHS were added to a concentration of 1 mM and 2.5 mM, respectively. This solution was agitated at room temperature for 15 min and then the pH was adjusted to 7 using NaOH. This pH change was to bring the solution back up into the optimal range for the EDC/NHS coupling reaction which is between pH 7-9. 2.2 mg/ml of aminated silica NPs were added to the solution and left to react overnight with agitation. The next day the NPs were washed with the same process used to wash the GABA-coated particles. The supernatants from each of the washes was saved so that the concentration of free glutamic acid could be quantified.

4.2.2 Determination of Glutamic Acid Conjugation using Fluorescamine Assay

The supernatant from each wash was retained and the amount of glutamic acid in each was measured using the fluorescamine assay. A range of standards was made from 0 to 0.2 mg/ml ethanolamine in water. 150 µl of each standard and wash was added to a black 96 well plate. 50 µl of 3 mg/ml fluorescamine in DMSO was added to each well and the solution was allowed to react for 10 minutes protected from light. Samples were excited at 400 nm and emissions were analyzed at 460 and 475 nm. Figure 7 shows a typical standard curve for this assay that was used to determine glutamic acid concentrations.

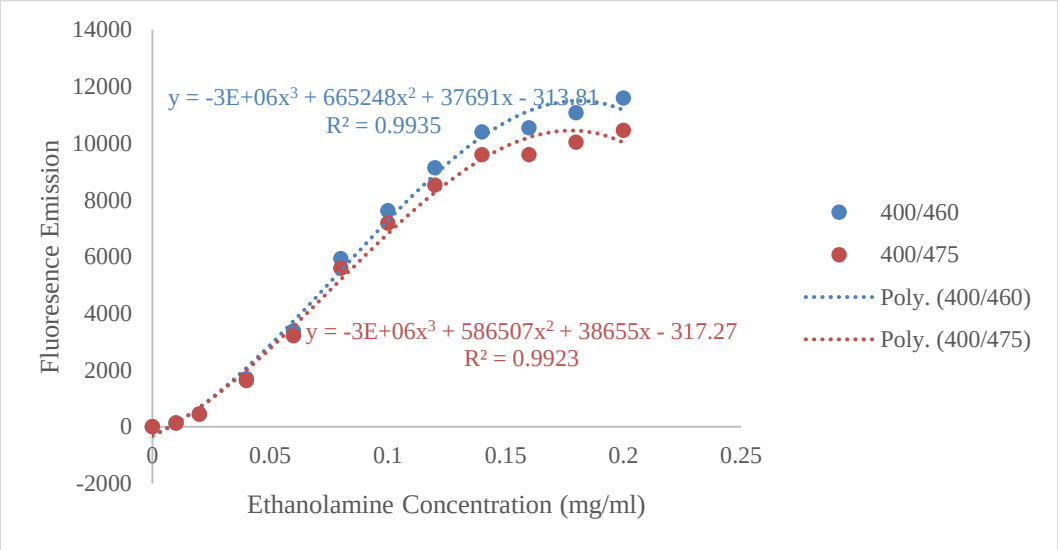

Figure 7. Standard curve for fluorescamine assay.

This curve was used to calculate the amount of glutamic acid in each of the washes to indirectly calculate how much glutamic acid had attached to the NPs. For each batch of glutamic acid-coated NPs made, the values measured suggest that more than 100% of the available amines on the surface of the NPs had bound with glutamic acid. This suggests that the glutamic acid was reacting with both itself and the NPs, forming chains. 259% of

the available amines were bound with the first batch of NPs. The following batch showed 700% bound which further supported this conclusion.

It is possible that the process of allowing the glutamic acid and EDC and NHS to react before introducing the nanoparticles was pushing the glutamic acid to form chains during the 15 min agitation period. Therefore, the protocol was repeated with separate batches prepared only at pH 3 or 7 to determine if pH played a large role on attachment. Fluorescamine assay showed that 499±8% of the available amines were bound when the reaction was run at pH 3, and 479±8% was bound when the reaction was performed at pH 7. Because greater attachment was attained at pH 3, the protocol was changed to run the reaction entirely at pH 3.

4.2.3 FTIR Analysis of Glutamic Acid-Coated Nanoparticles

Fourier transform infrared spectroscopy (FTIR) was used to investigate if glutamic acid was successfully attached to the Si NPs. Figure 8 shows the FTIR spectra for glutamic acid, aminated silica NPs, and glutamic acid-coated silica NPs, each ran using a potassium bromide (KBr) background.

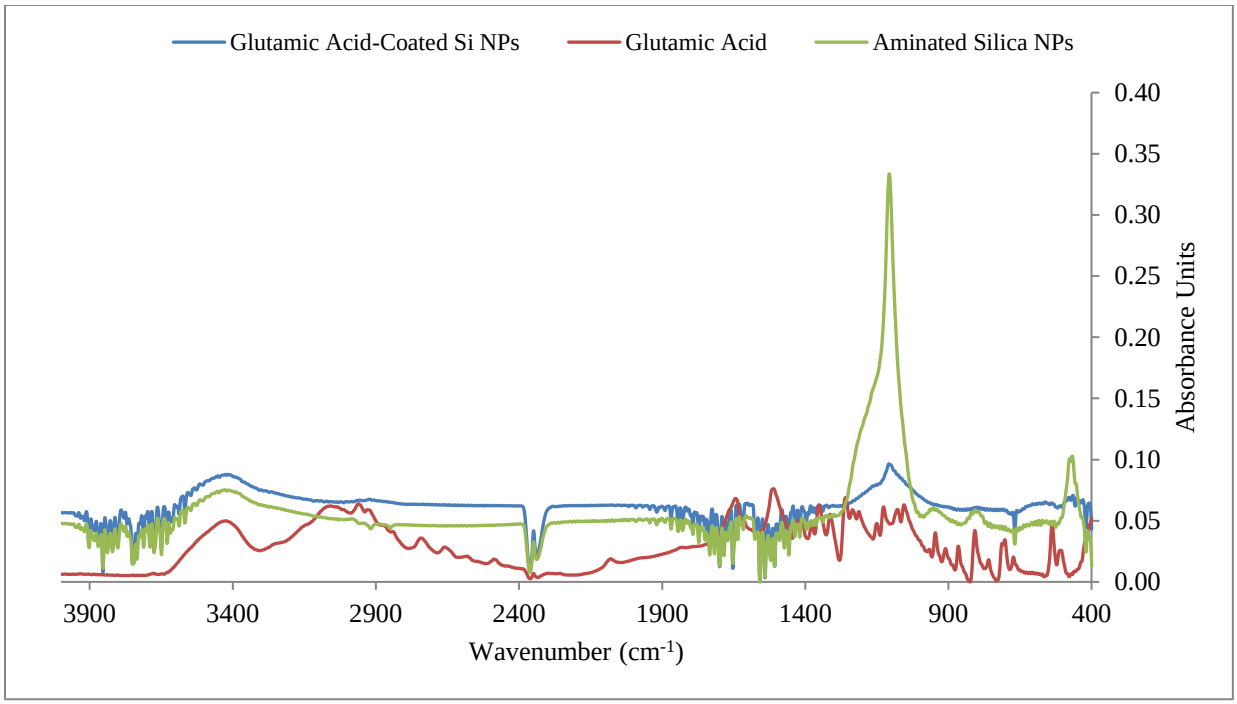

Figure 8. FTIR spectra for glutamic acid-coated NPs and their components.

The spectra for the coated and aminated particles line up well, but it is more difficult to align peaks between the coated particles and the free glutamic acid spectrum. This may be due to the fact that the ratio of silica present to glutamic acid present in the coated NPs was so high that the Si spectra greatly outweighed any peaks from the glutamic acid. Alternatively, there may be attached glutamic acid but not in a large enough quantity to cause a significant peak.

4.2.4 DLS and Zeta Potential Measurements for Particle Characterization

Dynamic light scattering (DLS) was performed to investigate what effect the glutamic acid conjugation had on the particles. Figure 9 shows a typical DLS distribution for the glutamic acid-coated particles in two dispersants, deionized H_2O and HEPES.

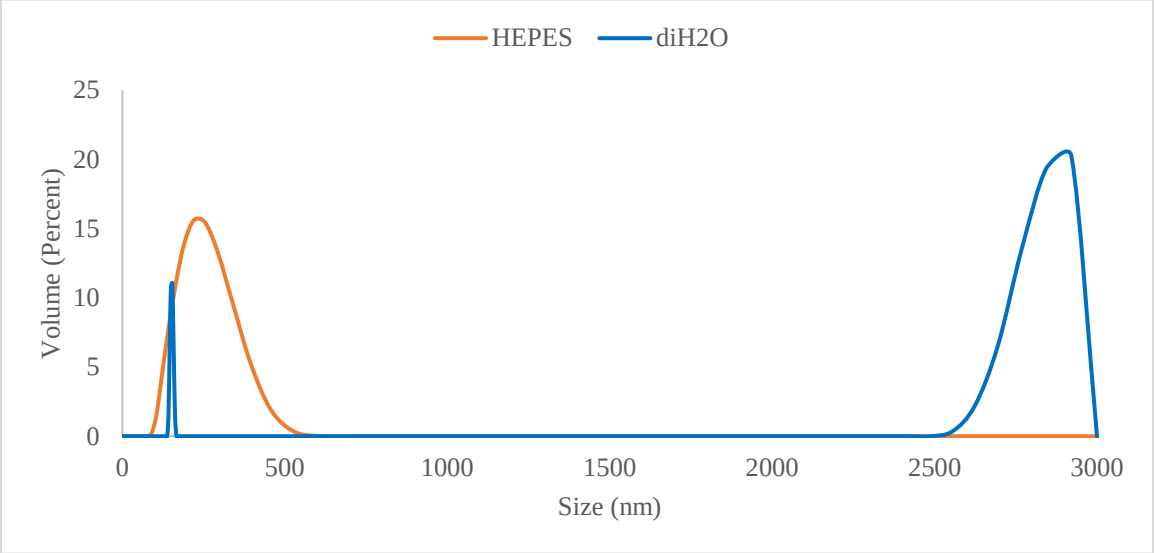

Figure 9. DLS analysis of glutamic acid-coated Si NPs.

In deionized H_2O, there is a spike around 120 nm that suggests some of the original 120 nm particles are still free, the peak in the 2900 nm range suggests that many of the particles have aggregated. Each sample was vortexed for several seconds before the DLS reading was taken, so it is most likely that the particles have bound together through the glutamic acid bridging. Upon transferring the NPs to HEPES buffer, the aggregation peak disappears, but the peak around 120 nm widens. The NPs contain both positive and negative charges on their surface, which may attract the HEPES molecule, which also contains positive and negative charges in its functional groups. This could result in an association of HEPES on the surface of the particles. In future work, this reaction will need to be curtailed in order to avoid this type of conglomeration.

The zeta potential (ζ) of the glutamic acid-coated NPs was also measured and compared with that of the unaltered aminated Si NPs. Coated NPs were initially suspended in deionized H_2O, however the particles visibly fell out of solution after

several minutes which indicated they were not stable in this dispersant. Therefore, 20mM 4-(2-hydroxyethyl)-1-piperazineethanesulfonic acid) (HEPES) was used as the dispersant. The particles were stable over a longer period of time in HEPES buffer, so ζ measurements were carried out using HEPES. Table 4 gives the ζ measurements for both aminated Si NPs and glutamic acid-coated Si NPs.

Table 4. Comparison of zeta potential of aminated Si NPs and glutamic acid-coated Si NPs.

Nanoparticle	ζ (mV)
Aminated Silica NPs	34.5 ± 0.5
Glutamic Acid-Coated Silica NPs	37.2 ± 0.9

The zeta potential of the glutamic acid-coated NPs is noticeably larger than that of the aminated Si NPs. This can be explained by the presence of carboxylic acid groups on the glutamic acid-coated particles which increase the potential difference between the slipping plane surrounding the particle and the dispersant. This difference suggests an electrophysiological difference between the two particles types, indicating some degree of successful conjugation of glutamic acid to the surface of the aminated Si NPs.

4.3 Investigation of Activated Neuronal Receptors

The receptor of interest for these targeted NPs, the GABA receptor, is associated with neuronal inhibition. This is due to GABA's effect on the influx of negative chloride ions. Upon activation of the GABA receptor, chloride ions rush into the cell and hyperpolarize the neuron, thus increasing the threshold necessary for firing and inhibiting activation of the neuron. Neurons will fire an action potential when the cell has been sufficiently depolarized, so the further hyperpolarization of the cell by GABA-mediated

chloride influx increases the amount of depolarization necessary to reach this condition [63]. Thus, the effect of the glutamic acid-coated NPs on chloride channel conductance is of interest.

4.3.1 Study of Chloride Activation by Coated NPs in GABAergic Cells

Two cells lines were used for study, the SH-SY5Y human neuroblastoma cell line which is GABAergic, or GABA-containing, and Chinese hamster ovary cell line (CHO) which is non-GABAergic. SH-SY5Y cells were seeded at a density of $7x10^4$ cells/well and CHO cells were seeded at a density of $4x10^4$ cells/well to ensure that both cultures reached 80-90% confluency the following day. Six wells of cells were seeded per condition. Using a chloride assay, the amounts of chloride present in both cells lines in the presence of a high "dosage" of glutamic acid-coated NPs, a low "dosage", and no NPs was measured. The high and low dosages, 0.3 mg/ml and 0.075 mg/ml, were based on typical dosages of gabapentin when prescribed for chronic pain. Six wells of cells were created for each condition. The cell media was aspirated off and 50 µl of chloride-free PBS was added to each well, followed by 150 µl of the chloride reagent provided by BioVision's Chloride Colorimetric Assay Kit mixed with the appropriate amount of NPs. The absorbance of each sample was immediately measured at 620 nm over 14 s following addition of the reagent. Figure 10 shows the chloride levels for each condition.

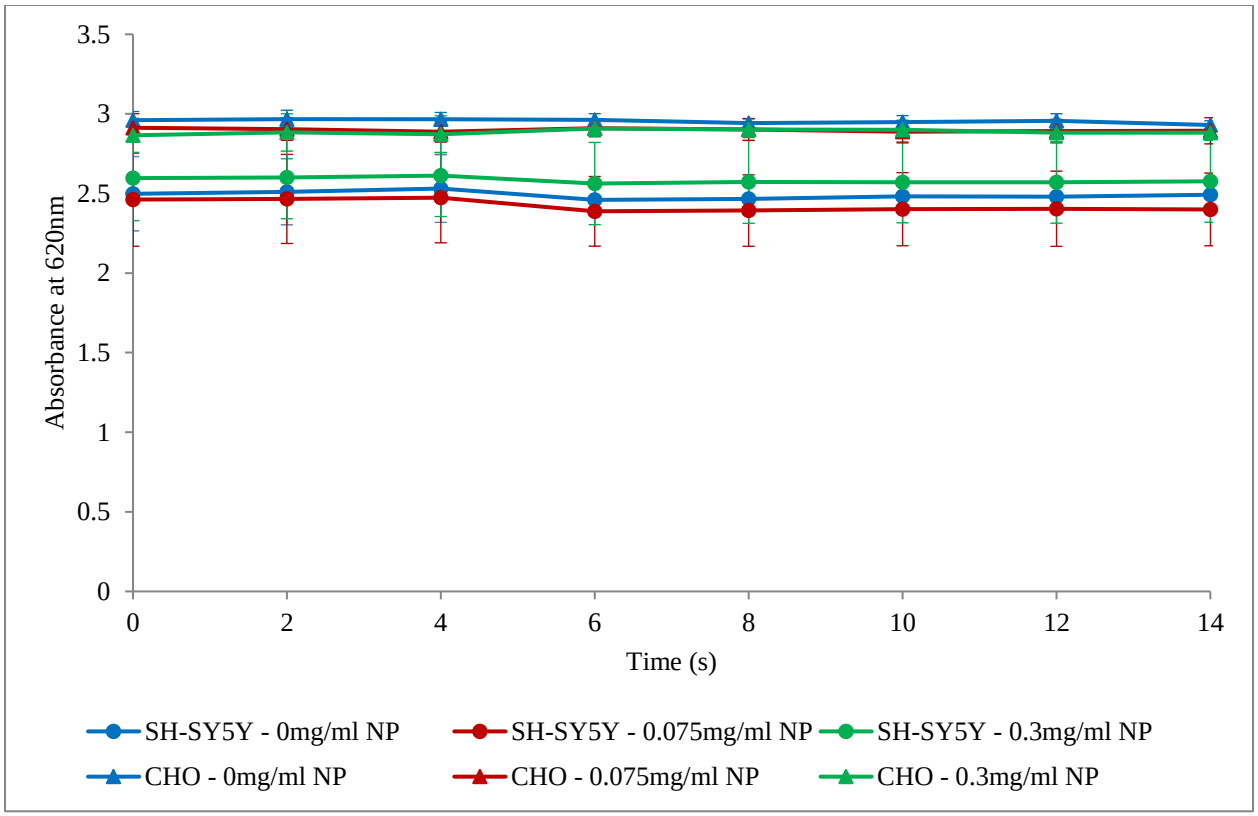

Figure 10. Comparison of chloride levels present in SH-SY5Y and CHO cells lines in the presence of various levels of glutamic acid-coated Si NPs.

There is no statistical difference in chloride level between the two cell lines or between the levels of coated NPs present, which suggests that the GABA receptors are not being activated. This could be due to a number of factors including steric hindrance due to the arrangement of glutamic acid on the NP surface, or the amount of glutamic acid mimicking GABA was not at a biologically relevant level.

4.3.2 Study of Potassium and Calcium Activation by Coated NPs in GABAergic Cells

While the NPs were subjected to three rounds of washing, it is possible that some residual unbound glutamic acid made it through to the final formulation. This could lead to the activation of other receptor types found in neurons, namely the α-amino-3-hydroxy-5-methyl-4-isoxazolepropionic acid receptor (AMPAR) and the N-methyl-D-aspartate receptor (NMDAR). AMPARs are involved in the mediation of fast synaptic transmission in mature CNS neurons typically responsible for excitation and are agonized by glutamate, the deprotonated form of glutamic acid [64]. Upon activation, the AMPAR's potassium and sodium permeability increases, allowing these positively charged ions to flow into the neuron, depolarizing it [65]. If the cell is depolarized above its firing threshold, then the neuron will generate an action potential to propagate the received signal on through the network of CNS neurons. The NMDARs are also ionotropic glutamate receptors, but they allow not only an influx of potassium and sodium upon activation, but also calcium influx [66], [67]. While AMPARs lacking the GluR2 subunit will be permeable to calcium, the majority of these receptors in the adult CNS contain this subunit, making a clear distinction between the gating actions of AMPA and NMDA receptors [68]. Therefore, similar assays to the chloride assay discussed previously were performed to investigate if the glutamic acid-coated NPs had any effect on the behavior of the AMPARs and NMDARs.

The same experimental setup was used for both assays, with a high and low "dosage" of NPs tested as well as a negative control without NPs between the SH-SY5Y GABAergic cells and the non-GABAergic CHO cells, with six replicates per condition.

The FLIPR Potassium Assay Kit was purchased from Molecular Devices for the measurement of potassium channel activity. Media was aspirated from the cells and 100 µl of Hank's Balanced Salt solution (HBSS) and 100 µl of the loading buffer provided were added to each well. The plate was incubated for 1 hour at room temperature and then a 3 mM thallium sulfate solution was added and the fluorescence of the wells at an excitation wavelength of 485 nm and an emission wavelength of 525 nm was measured over five minutes, with a 2 s sampling rate. Figures 11 and 12 show the trends over time of the two cells types in the presence of various levels of the glutamic acid-coated NPs.

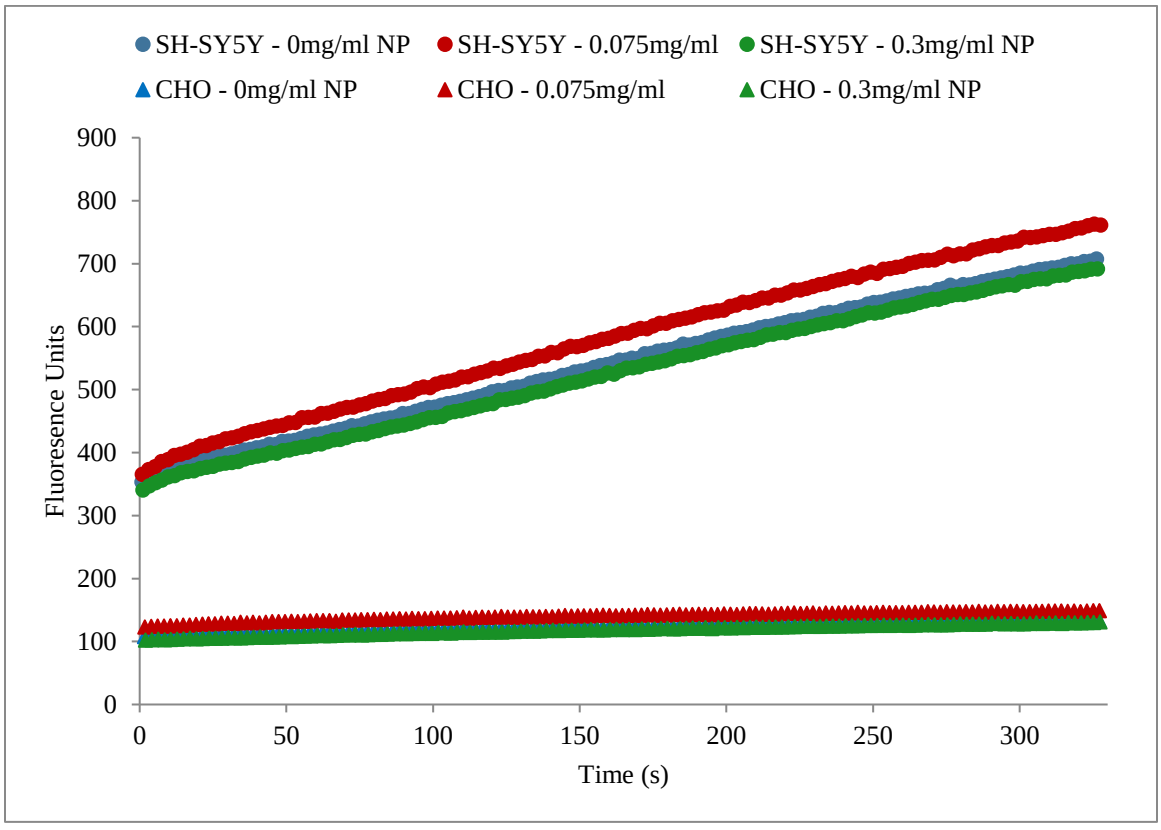

Figure 11. Comparison of potassium channel activity for GABAergic and non-GABAergic cells in the presence of glutamic acid-coated Si NPs. (Error bars not shown)

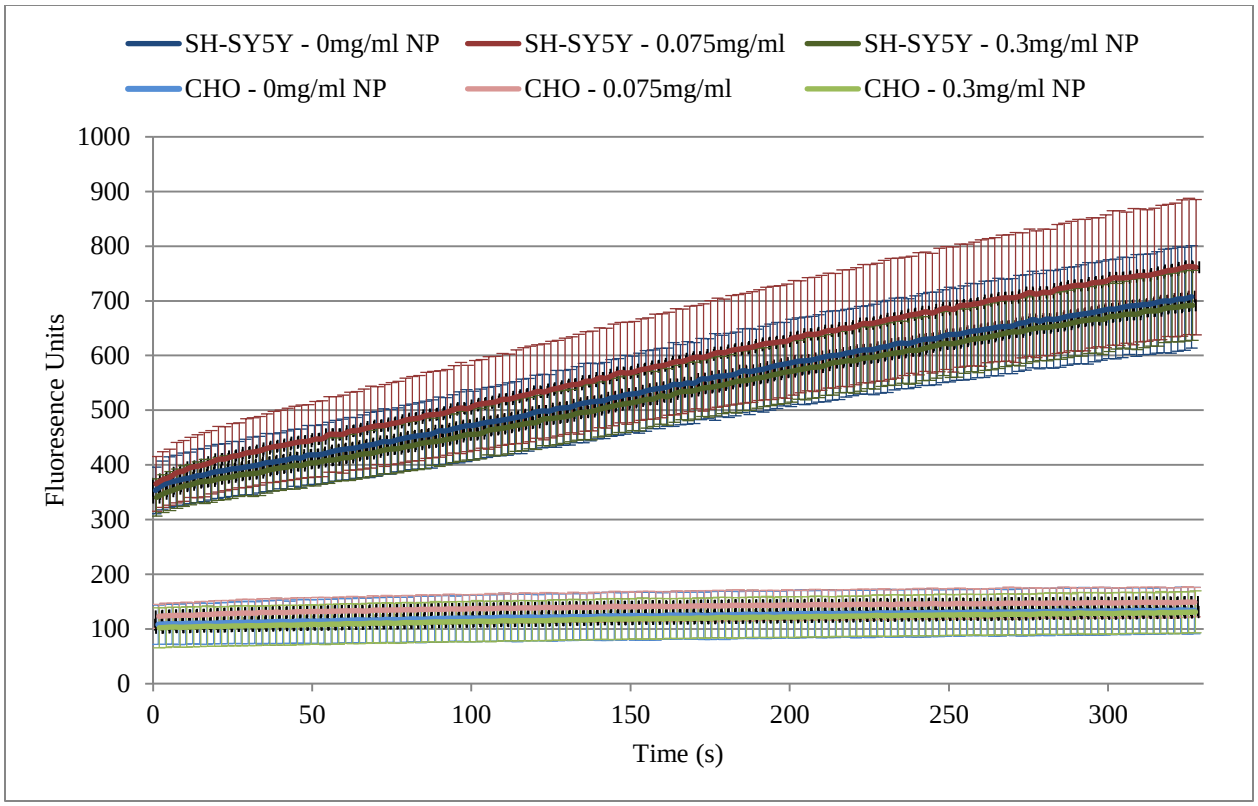

Figure 12. Comparison of potassium channel activity for GABAergic and non-GABAergic cells in the presence of glutamic acid-coated Si NPs.

While the behavior between the two cell lines was statistically significant, there was no appreciable difference in potassium activity at the various NP dosages in the GABAergic cells. This could be due to human error, as the automation function on the spectrophotometer which was meant to transfer the thallium sulfate solution was malfunctioning. This meant the thallium sulfate was added by hand and then the plate inserted into the machine, preventing immediate data points from being collected, as well as introducing pipetting errors into the system. This study should be repeated using the automatic liquid transfer function of the spectrophotometer to determine if the large error was associated with human error or if the NPs had no effect on the GABAergic cells.

A similar outcome occurred with the assay to measure calcium mobilization in the presence of the glutamic acid-coated NPs. Cell media was aspirated off and 100 µl of the loading dye provided in the FluoForte Calcium Assay kit from Enzo was added. The plate was incubated for 15 min at room temperature, and then the appropriate NP solutions were added to each well. The samples were excited with an excitation wavelength of 490 nm and an emission wavelength of 525 nm over 5 min, with a reading taken every 2 s for every sample. Figures 13 and 14 compare the amount of intracellular calcium between the SH-SY5Y and CHO cells in the presence of various levels of NPs.

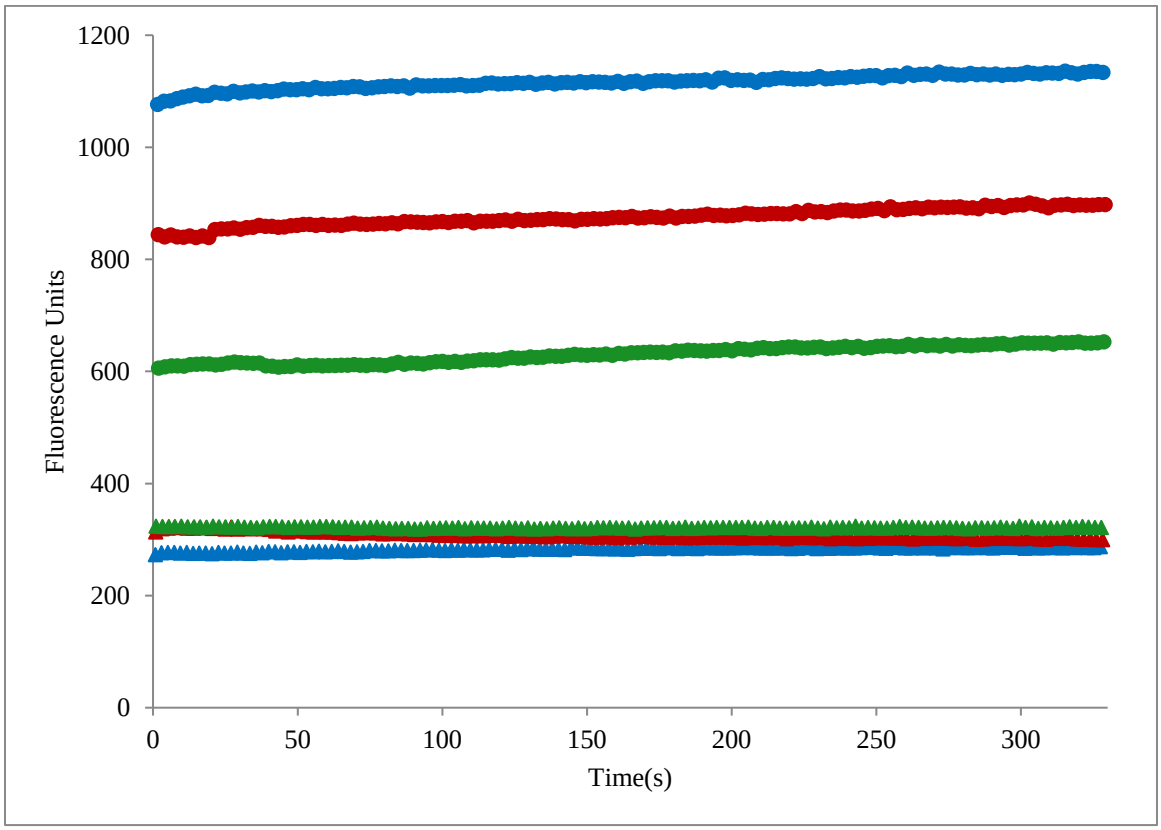

Figure 13. Comparison of intracellular calcium for GABAergic and non-GABAergic cells in the presence of glutamic acid-coated NPs. (Error bars not shown)

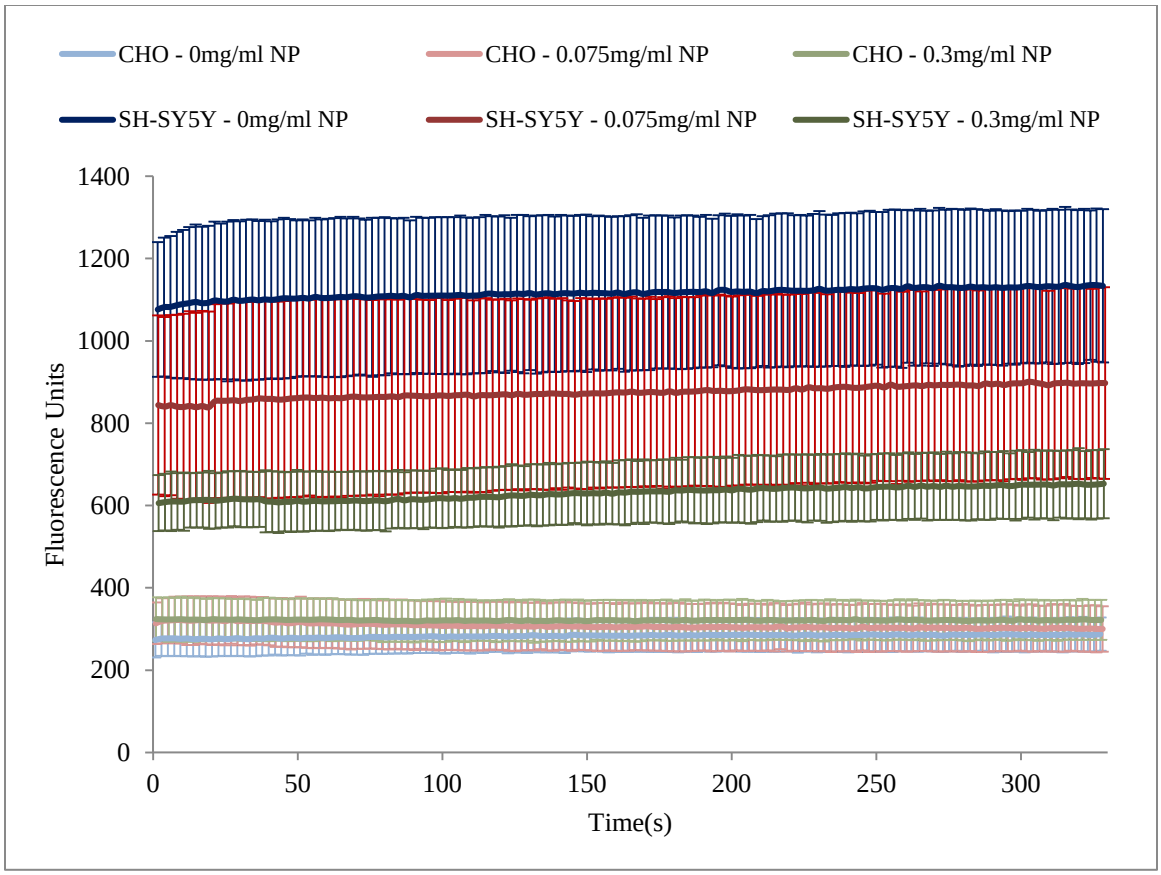

Figure 14. Comparison of intracellular calcium for GABAergic and non-GABAergic cells in the presence of glutamic acid-coated NPs.

In the case of intracellular calcium, there is a difference in behavior observed between the SH-SY5Y neuroblastomas treated with the high dosage of NPs as compared to the condition with no NPs ($p < 0.001$). This suggests that the glutamic acid-coated NPs have an effect on calcium ion gating in neuronal cells. Of the three receptors previously discussed, only the NMDA receptor is involved in the control of calcium ion flow. However, upon activation, the NMDA receptor will allow an influx of calcium; however, above shows a decrease in intracellular calcium with the addition of the NPs. This suggests that the NPs are having an effect on one or a combination of other receptors, which may include the NMDA receptors, which can control calcium ion flow. Further

investigation will be needed to elucidate exactly what combination of calcium gating receptors are being affected. This assay shows that the glutamic acid-coated particles do have some effect on neuronal cells.

4.4 Simulations of GABA Effects on Neural Networks in the Hippocampus

A network of 100 cells modeling a section of the hippocampus was developed, as described in Section 3.13. This network was comprised of 10 interneurons and 90 pyramidal neurons divided into three subclasses with varying parameters to simulate the heterogenous hippocampal environment. A shock and a tone were introduced into the system for 2000 ms via the interneurons to simulate typical incoming stimuli from the thalamus and cortex. Figure 13 shows the resulting network of cells and randomly generated connections.

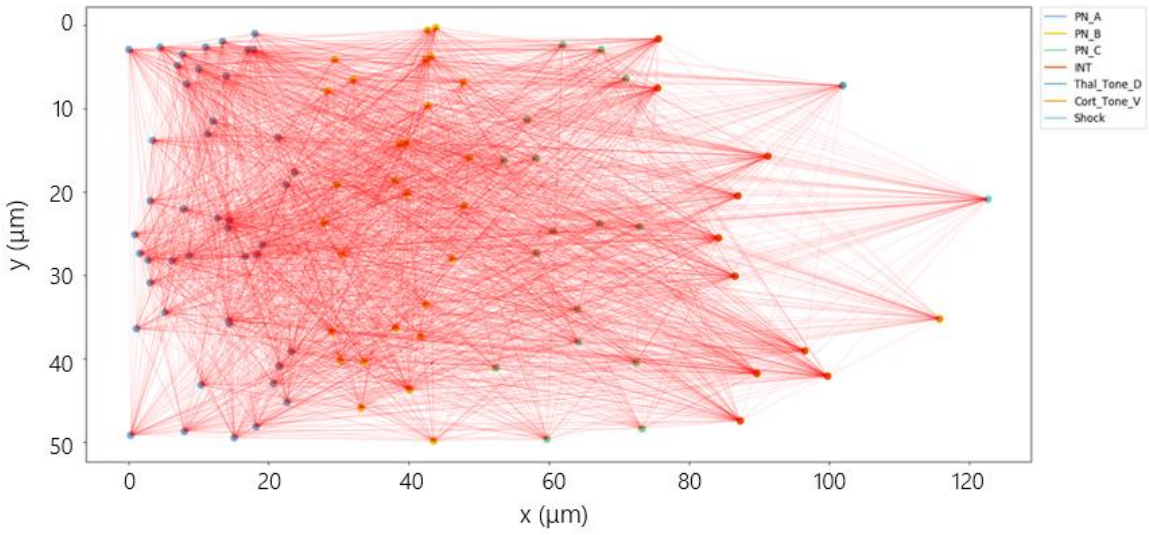

Figure 15. Neural network model of the hippocampus receiving stimuli from the thalamus and cortex.

The voltage change over 2000 ms was recorded for every cell in the network. Figures 14 shows voltage versus time graph for a random cell of each cell class in the model.

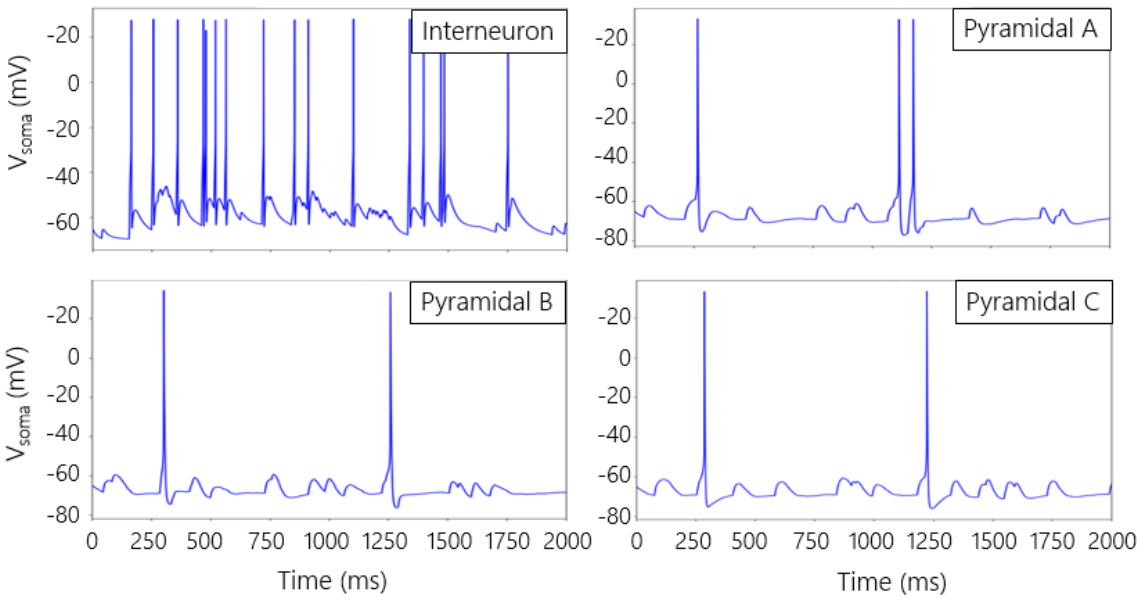

Figure 16. Firing patterns in pyramidal neuron subclasses and interneurons in a typical hippocampal environment.

While these graphs are not indicative of the exact behavior of each cell throughout the network, there is a clear distinction in behavior between the pyramidal neurons and interneurons. The interneurons are propagating signals much more rapidly, whereas the various pyramidal cells only fire a few times over the course of the stimulation. This makes sense, as the function of interneurons is to relay signals between different neuronal cell types. As the signal is propagated through the network, the intensity of the signal diverges between the cells in the network and is diminished, resulting in less frequent firing in the pyramidal neurons. Figure 15 is a raster plot which maps out which cells fire when over the 2000 ms stimulation period.

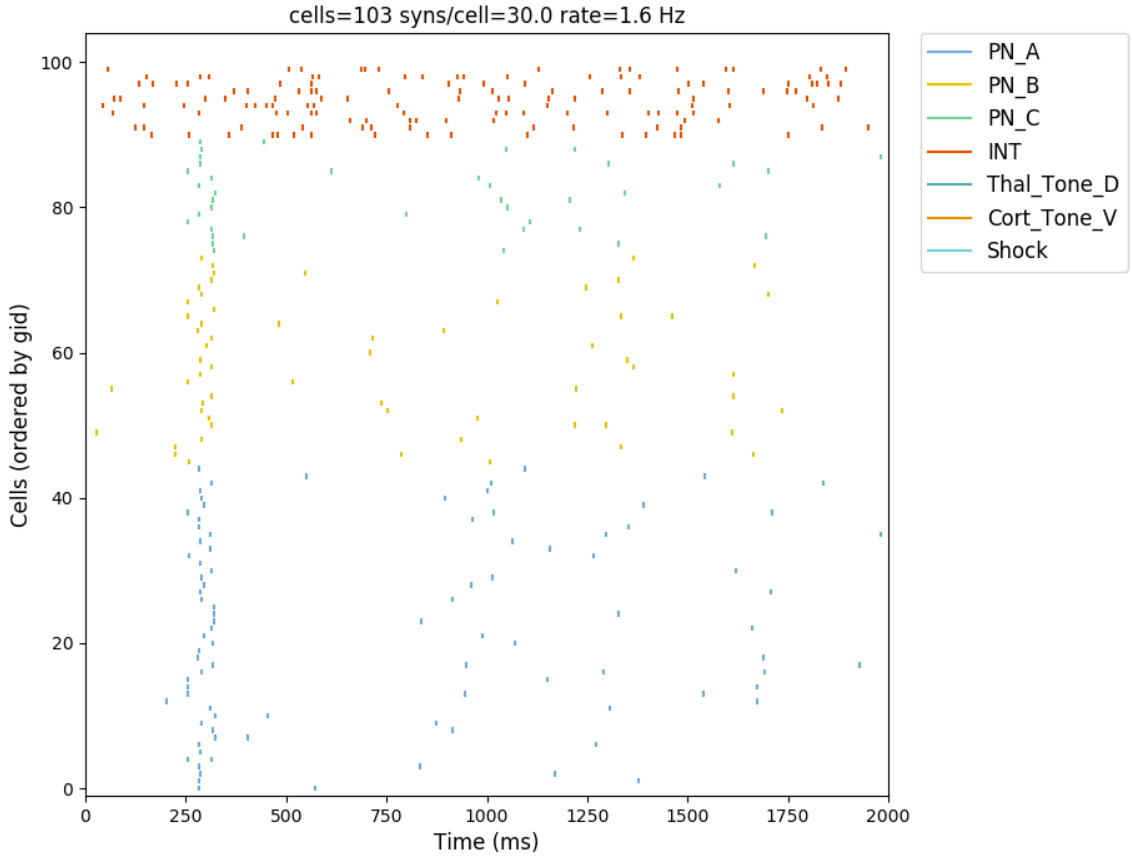

Figure 17. Timing of individual cell firing events over 2000 ms.

To model the effect that GABA would have on the hippocampus, several parameters were altered in the model based on literature reports of the effect of GABA on cell properties. GABA primarily behaves as an inhibitory neurotransmitter in mature adult neurons. It inhibits the firing of action potentials using chloride ions. When activated, the GABA receptors will open and allow an influx of negative chloride ions which further polarize the cell. Thus, the threshold for firing increases, as more positively charged ions are now necessary to overcome the initial voltage potential plus the presence of the negative chloride ions. This causes the cell to fire less frequently, or not at all [61], [69]. This was modeled using the same hippocampus-based network by

making the resting voltage potential of the pyramidal neurons and interneurons more negative. The resulting firing patterns of the same four cells are shown in Figure 16.

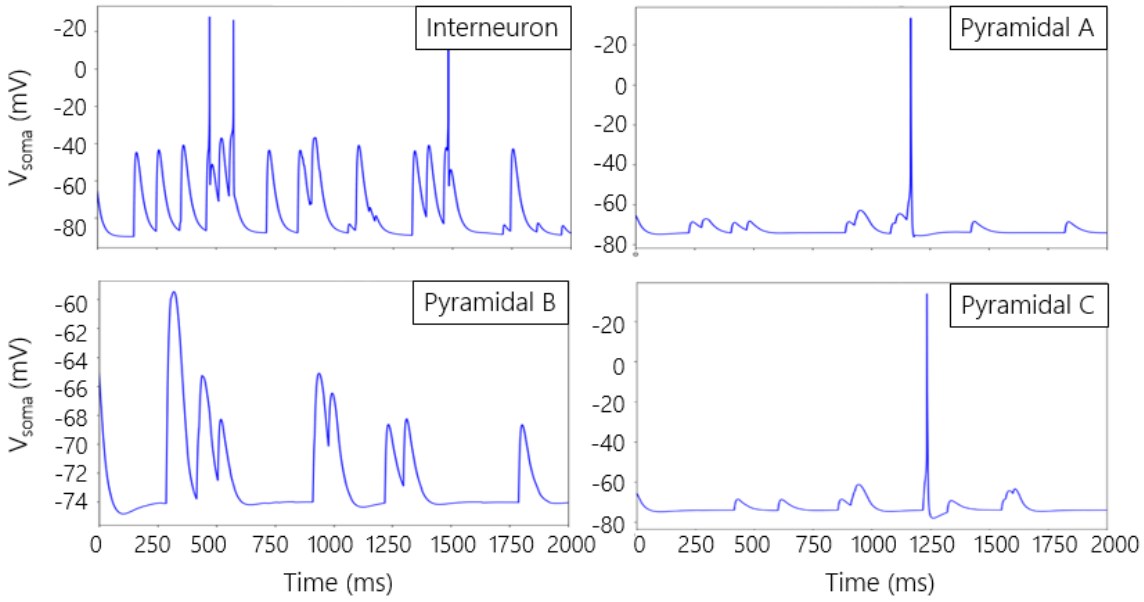

Figure 18. Firing patterns in pyramidal neuron subclasses and interneurons in the presence of GABA.

It can be seen from the figures that GABA has a drastic effect on the ability of the interneurons to fire, resulting in a decrease in firing frequency in the pyramidal neurons. Cell A and C only receive a large enough signal to fire once, and Cell B is never able to surpass its firing threshold. The decrease in action potential generation across the network can be visualized in Figure 17.

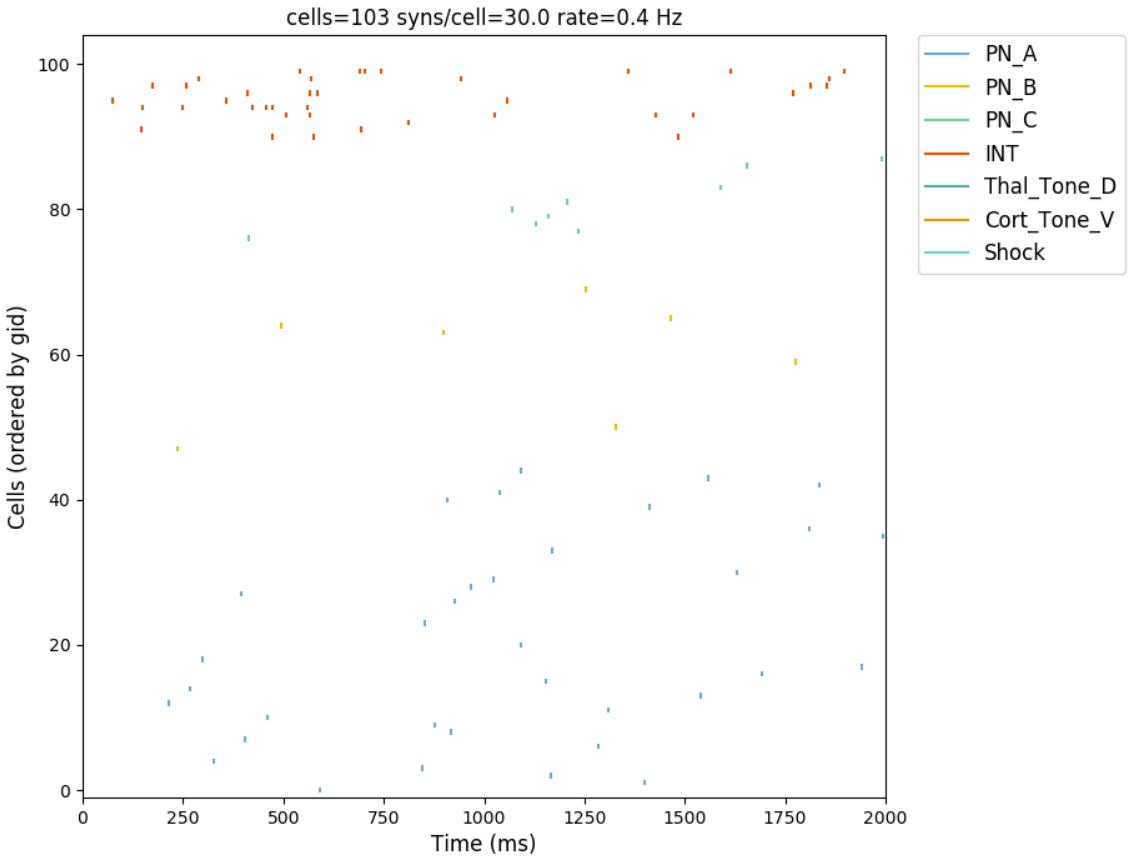

Figure 19. Timing of individual cell firing events in the presence of GABA.

This figure serves to demonstrate the drastic inhibitory effect that GABA can have on a network of various neuron types. This response is the ideal outcome for a neural network propagating pain signals after the application of targeted silica nanoparticles, and moving forward, this model will serve as a guide for the ideal outcome and also understanding of the effect of targeted NPs on a neural network responsible for pain signal propagation.

Chapter 5

Conclusions and Recommendations

The utility of nanoparticles has been proven repeatedly in a variety of applications over the past several decades. With the experiments outlined here, the formulation of a 120 nm silica NP coated with glutamic acid that can specifically target the receptors found in mature neurons involved in the signaling of pain shows promise. The results from the receptor activation studies suggest that a repeated trial, this time using a spectrophotometer with functional automated liquid transfer, would further elucidate the effect that NPs coated in glutamic acid have on neuronal cells which express the GABA, AMPA, and NMDA receptor types. Additionally, further assays should be performed to investigate other receptors that are involved in calcium ion flow. Better understanding of these mechanisms will allow smarter formulations to be developed. Ideas for other surface modifying molecules may be inspired by studying the structure of other neurotransmitters and how they interact with neuronal receptors. Additionally, the search should be widened to molecules that are not classical neurotransmitters but still interact with the nervous system. For example, Malerba et al. developed a form of the neurotrophin human nerve growth factor (NGF) which shows high nociceptive action [70]. Molecules such as these should be studied to better understand how molecules are interacting with and disrupting the propagation of various types of pain signaling.

Upon the development of a NP which shows significant effect on the receptors of interest, the models developed with the NEURON software may serve as a guide for ideal results in a laboratory setting. Current clamp recordings may be performed on GABAergic neurons in the presence of the developed NP in an effort to match the models of GABA-mediated inhibition of signal propagation. Furthermore, the NEURON package allows for more models to be developed, including the effect of a nanoparticle which would behave not as an inhibitory neurotransmitter, but as an excitatory one.

The combination of intelligently designed NP surface modifications based on molecules which interact with the nervous system along with simulations that model a desirable laboratory outcome will serve to guide this project to the development of a NP which selectively targets mature neurons involved in the propagation of a chronic pain response in a safe and non-addictive manner. This, in turn, stands to drastically change the way that chronic pain is managed in millions of patients across a wide variety of demographics.

References

Bibliography

[1] T. N. Academies, “Relieving Pain in America: A Blueprint for Transforming Prevention, Care, Education, and Research,” 2016.

[2] T. S. Jensen, R. Baron, M. Haanpaa, E. Kalso, J. D. Loeser, A. S. C. Rice, and R. D. Treede, “A new definition of neuropathic pain,” *Pain*, vol. 152, no. 10, pp. 2204–2205, 2011.

[3] R. Baron, A. Binder, and G. Wasner, “Neuropathic pain: Diagnosis, pathophysiological mechanisms, and treatment,” *Lancet Neurol.*, vol. 9, no. 8, pp. 807–819, 2010.

[4] M. C. Woodle, “Sterically stabilized liposome therapeutics,” *Adv. Drug Deliv. Rev.*, vol. 16, no. 2–3, pp. 249–265, 1995.

[5] A. C. Anselmo and S. Mitragotri, “Cell-mediated delivery of nanoparticles: Taking advantage of circulatory cells to target nanoparticles,” *J. Control. Release*, vol. 190, pp. 531–541, 2014.

[6] F. Rossi, R. Ferrari, S. Papa, D. Moscatelli, T. Casalini, G. Forloni, G. Perale, and P. Veglianese, “Tunable hydrogel-Nanoparticles release system for sustained combination therapies in the spinal cord,” *Colloids Surfaces B Biointerfaces*, vol. 108, pp. 169–177, 2013.

[7] Y. S. Choi, M. Y. Lee, A. E. David, and Y. S. Park, “Nanoparticles for gene delivery: therapeutic and toxic effects,” *Mol. Cell. Toxicol.*, vol. 10, no. 1, pp. 1–8, 2014.

[8] G. Bao, S. Mitragotri, and S. Tong, “Multifunctional nanoparticles for drug delivery and molecular imaging.,” *Annu. Rev. Biomed. Eng.*, vol. 15, pp. 253–82, 2013.

[9] R. H. Dworkin, A. B. O. Connor, M. Backonja, J. T. Farrar, N. B. Finnerup, T. S. Jensen, E. A. Kalso, J. D. Loeser, C. Miaskowski, T. J. Nurmikko, R. K. Portenoy, A. S. C. Rice, B. R. Stacey, R. Treede, D. C. Turk, and M. S. Wallace, “Pharmacologic management of neuropathic pain : Evidence-based recommendations,” vol. 132, pp. 237–251, 2007.

[10] D. C. U'Prichard, D. A. Greenberg, P. P. Sheehan, and S. H. Snyder, "Tricyclic Antidepressants : Therapeutic Properties and Affinity for α-Noradrenergic Receptor Binding Sites in the Brain," *Science (80-.).*, vol. 199, no. 4325, pp. 197–198, 1978.

[11] M. Zhuo, "Neuronal Mechanism for Neuropathic Pain," *Mol. Pain*, vol. 3, no. 14, 2007.

[12] L. D. C. Mannelli, L. Micheli, L. Crocetti, M. P. Giovannoni, C. Vergelli, and C. Ghelardini, "α 2 Adrenoceptor: A Target for Neuropathic Pain Treatment," *Mini Rev Med Chem*, vol. 6, pp. 95–107, 2017.

[13] I. Gilron, J. Bailey, D. Tu, and R. Holden, "Nortriptyline and gabapentin, alone and in combination for neuropathic pain: a double-blind, randomised controlled crossover trial," *The Lancet*. pp. 1252–1261, 2009.

[14] C. H. Wilder-Smith, B. S. Hill, Lauren T, and M. D. Laurent, Sophie, "Postamputation Pain and Sensory Changes in Treatment-naive Patients," *Anesthesiology*, vol. 103, no. 3, pp. 619–628, 2005.

[15] W. A. Ray, S. Meredith, P. B. Thapa, K. Hall, and K. T. Murray, "Cyclic antidepressants and the risk of sudden cardiac death," *Clin. Pharmacol. Ther.*, vol. 75, no. 3, pp. 234–241, 2004.

[16] A. R. Gammaitoni and M. W. Davis, "Pharmacokinetics and tolerability of lidocaine patch 5% with extended dosing," *Ann. Pharmacother.*, vol. 36, no. 2, pp. 236–240, 2002.

[17] A. Kanai, A. Suzuki, M. Kobayashi, and S. Hoka, "Intranasal lidocaine 8% spray for second-division trigeminal neuralgia," *Br. J. Anaesth.*, vol. 97, no. 4, pp. 559–563, 2006.

[18] H. L. Fields, "NeuroView The Doctor ' s Dilemma : Opiate Analgesics and Chronic Pain NeuroView," *Neuron*, vol. 69, no. 4, pp. 591–594, 2011.

[19] N. B. Finnerup, S. H. Sindrup, and T. S. Jensen, "The evidence for pharmacological treatment of neuropathic pain," *Pain*, vol. 150, no. 3, pp. 573–581, 2010.

[20] C. Norrbrink and M. Lofgren, "Needs and requests - patients and physicians voices about improving the management of spinal cord injury neuropathic pain," *Disabil. Rehabil.*, vol. 38, no. 2, pp. 151–158, 2016.

[21] M. A. Caudill-Slosberg, L. M. Schwartz, and S. Woloshin, "Office visits and analgesic prescriptions for musculoskeletal pain in US: 1980 vs. 2000," *Pain*, vol.

109, no. 3, pp. 514–519, 2004.

[22] M. J. Edlund, D. Steffick, T. Hudson, K. M. Harris, and M. Sullivan, “Risk factors for clinically recognized opioid abuse and dependence among veterans using opioids for chronic non-cancer pain,” *Pain*, vol. 129, no. 3, pp. 355–362, 2007.

[23] J. C. Ballantyne and K. S. LaForge, “Opioid dependence and addiction during opioid treatment of chronic pain,” *Pain*, vol. 129, no. 3, pp. 235–255, 2007.

[24] E. Kalso, J. E. Edwards, R. A. Moore, and H. J. McQuay, “Opioids in chronic non-cancer pain: systematic review of efficacy and safety,” *Pain*, vol. 112, no. 3. pp. 372–380, 2004.

[25] G. Pickering, M. Marcoux, S. Chapiro, L. David, P. Rat, M. Michel, I. Bertrand, M. Voute, and B. Wary, “An Algorithm for Neuropathic Pain Management in Older People,” *Drugs Aging*, vol. 33, no. 8, pp. 575–583, 2016.

[26] L. E. Chaparro, P. J. Wiffen, R. A. Moore, and I. Gilron, “Combination pharmacotherapy for the treatment of neuropathic pain in adults,” *Cochrane Database Syst. Rev.*, 2012.

[27] C. L.E., W. P.J., M. R.a., and G. I., “Combination pharmacotherapy for the treatment of neuropathic pain in adults,” *Cochrane Database Syst. Rev.*, vol. 7, no. 7, p. CD008943, 2012.

[28] S. Rama, M. Zbili, and D. Debanne, “Modulation of spike-evoked synaptic transmission: The role of presynaptic calcium and potassium channels,” *Biochim. Biophys. Acta - Mol. Cell Res.*, vol. 1853, no. 9, pp. 1933–1939, 2014.

[29] R. Van Seventer, H. A. Feister, J. P. Y. Jr, and M. Stoker, “Efficacy and tolerability of twice-daily pregabalin for treating pain and rel ...,” 2006.

[30] M. Hanna, C. O’Brien, and M. C. Wilson, “Prolonged-release oxycodone enhances the effects of existing gabapentin therapy in painful diabetic neuropathy patients,” *Eur. J. Pain*, vol. 12, no. 6, pp. 804–813, 2008.

[31] R. Baron, V. Mayoral, G. Leijon, A. Binder, I. Steigerwald, and M. Serpell, “Efficacy and safety of 5% lidocaine medicated plaster in comparison with pregabalin in patients with postherpetic neuralgia and diabetic polyneuropathy: Interim analysis from an open-label, two-stage adaptive, randomized, controlled trial,” *Clin. Drug Investig.*, vol. 25, no. 7, pp. 1677–1687, 2009.

[32] V. Challapalli, I. W. TremontLukats, E. D. McNicol, J. Lau, and D. B. Carr, “Systemic administration of local anesthetic agents to relieve neuropathic pain,” *Cochrane Database Syst. Rev.*, no. 4, 2005.

[33] C. J. Woolf and M. Costigan, “Transcriptional and posttranslational plasticity and the generation of inflammatory pain.,” *Proc. Natl. Acad. Sci. U. S. A.*, vol. 96, no. 14, pp. 7723–7730, 1999.

[34] L. Mason, R. A. Moore, S. Derry, J. E. Edwards, and H. J. Mcquay, “Systematic review of topical capsaicin for the treatment of chronic pain.,” *Br. Med. J.*, vol. 328, no. 7446, p. 991, 2004.

[35] J. P. Peesa, P. R. Yalavarthi, A. Rasheed, and V. B. R. Mandava, “A perspective review on role of novel NSAID prodrugs in the management of acute inflammation,” *J. Acute Dis.*, vol. 5, no. 5, pp. 364–381, 2016.

[36] R. Freeman, P. Raskin, D. J. Hewitt, G. J. Vorsanger, D. M. Jordan, J. Xiang, and N. R. Rosenthal, “Randomized study of tramadol/acetaminophen versus placebo in painful diabetic peripheral neuropathy.,” *Curr. Med. Res. Opin.*, vol. 23, no. 1, pp. 147–61, 2007.

[37] A. Tarantini, S. Huet, G. Jarry, R. Lanceleur, M. Poul, A. Tavares, N. Vital, H. Louro, M. J. Silva, and V. Fessard, “Genotoxicity of Synthetic Amorphous Silica Nanoparticles in Rats Following Short-Term Exposure. Part 1: Oral Route,” *Environ. Mol. Mutagen.*, vol. 56, pp. 218–227, 2015.

[38] H. Han, Y. Park, H. Park, and K. Lee, “Toxic and adjuvant effects of silica nanoparticles on ovalbumin-induced allergic airway inflammation in mice,” *Respiratory*, pp. 1–10, 2016.

[39] Y. Guichard, M.-A. Maire, S. Sebillaud, C. Fontana, C. Langlais, J.-C. Micillino, C. Darne, J. Roszak, M. Stepnik, V. Fessard, S. Binet, and L. Gate, “Genotoxicity of Synthetic Amorphous Silica Nanoparticles in Rats Following Short-Term Exposure, Part 2: Intratracheal Instillation and Intravenous Injection,” *Environ. Mol. Mutagen.*, vol. 56, pp. 228–244, 2015.

[40] D. C. Harris, “pH Measurement with a Glass Electrode,” in *Quantitative Chemical Analysis*, New York: W. H. Freeman and Company, 2016, pp. 347–349.

[41] D. C. Harris, “pH,” in *Quantitative Chemical Analysis*, New York: W. H. Freeman and Company, 2016, pp. 132–133.

[42] D. C. Harris, “Spectrophotometers,” in *Quantitative Chemical Analysis*, New York: W. H. Freeman and Company, 2016, pp. 491–492.

[43] D. C. Harris, “Luminescence,” in *Quantitative Chemical Analysis*, New York: W. H. Freeman and Company, 2016, pp. 448–451.

[44] D. C. Harris, “Fourier Transform Infrared Spectroscopy,” in *Quantitative*

Chemical Analysis, New York: W. H. Freeman and Company, 2016, pp. 514–516.

[45] R. B. Bird, W. E. Steward, and E. N. Lightfoot, "Theory of Diffusion in Binary Liquids," in *Transport Phenomena - Revised Second Edition*, John Wiley & Sons, Inc., 2007, pp. 528–529.

[46] R. W. O'Brien, B. R. Midmore, A. Lamb, and R. J. Hunter, "Electroacoustic Studies of Moderately Concentrated Colloidal Suspensions," *Faraday Discuss. Chem. Soc.*, vol. 90, pp. 301–312, 1990.

[47] C. E. Childs, "The Determination of Polyethylene Glycol in Gamma Globulin Solutions," *Microchem. J.*, vol. 20, pp. 190–192, 1975.

[48] Y. Chen and Y. Zhang, "Fluorescent Quantification of Amino Groups on Silica Nanoparticle Surfaces," *Anal. Bioanal. Chem*, vol. 399, pp. 2503–2509, 2011.

[49] Molecular Devices, "FLIPR ® Potassium Assay Kit," 2015.

[50] BioVision, "Chloride Colorimetrtic Assay Kit," 2013.

[51] Invitrogen, "Fluo-4 Direct ™ Calcium Assay Kits," 2009.

[52] N. T. Carnevale and M. L. Hines, "NEURON," 2013. [Online]. Available: https://www.neuron.yale.edu/neuron/.

[53] A. L. Hodgkin and A. F. Huxley, "A Quantitative Description of Membrane Current and Its Application to Conduction and Excitation in Nerve," *J. Physiol. - London*, vol. 117, pp. 500–544, 1952.

[54] S. Leknes and I. Tracey, "Hippocampus and Entorhinal Complex , Functional Imaging," *Encycl. Pain*, 2007.

[55] I. V. Viskontas, A. D. Ekstrom, C. L. Wilson, and I. Fried, "Characterizing Interneuron and Pyramidal Cells in the Human Medial Temporal Lobe In Vivo Using Extracellular Recordings," *Hippocampus*, vol. 17, pp. 49–57, 2007.

[56] F. Feng, P. Samarth, D. Paré, and S. S. Nair, "Mechanisms underlying the formation of the amygdalar fear memory trace: A computational perspective," *Neuroscience*, vol. 322, pp. 370–376, 2016.

[57] D. Kim, D. Paré, and S. S. Nair, "Mechanisms contributing to the induction and storage of Pavlovian fear memories in the lateral amygdala.," *Learn. Mem.*, vol. 20, no. 8, pp. 421–30, 2013.

[58] P. Tovote, J. P. Fadok, and A. Lüthi, "Neuronal circuits for fear and anxiety," *Nat. Publ. Gr.*, vol. 16, no. 6, pp. 317–331, 2015.

[59] D. I. B. Kerr and J. Ong, “GABAB receptors,” *Pharmacol. Ther.*, vol. 67, no. 2, pp. 187–246, 1995.

[60] J. Zhang, A. L. De Blas, C. P. Miralles, and C.-Y. Yang, “Localization of GABAA receptor subunits alpha 1, alpha 3, beta 1, beta 2/3, gamma 1, and gamma 2 in the salamander retina.,” *J. Comp. Neurol.*, vol. 459, no. 4, pp. 440–53, 2003.

[61] B. Birnir and E. R. Korpi, “The Impact of Sub-Cellular Location and Intracellular Neuronal Proteins on Properties of GABAA Receptors,” *Curr. Pharm. Des.*, vol. 13, pp. 3169–3177, 2007.

[62] A. T. Malouf, R. L. Schnaar, and J. T. Coyle, “Characterization of a glutamic acid neurotransmitter binding site on neuroblastoma hybrid cells,” *J. Biol. Chem.*, vol. 259, no. 20, pp. 12756–12762, 1984.

[63] R. W. Olsen and T. M. DeLorey, “GABA Receptor Physiology and Pharamcology,” in *Basic Neurochemistry: Molecular, Cellular and Medical Aspects*, 6th ed., Philadelphia: Lippincott-Raven, 1999.

[64] F. Fonnum, “Glutamate: A Neurotransmitter in Mammalian Brain,” *J. Neurochem.*, vol. 42, no. 1, pp. 1–11, 1984.

[65] D. Bredt and R. a Nicholl, “AMPA receptor trafficking at excitatory synapses,” *Neuron*, vol. 40, no. 2, pp. 361–379, 2003.

[66] G. Köhr, “NMDA receptor function: Subunit composition versus spatial distribution,” *Cell Tissue Res.*, vol. 326, no. 2, pp. 439–446, 2006.

[67] P. Paoletti and J. Neyton, “NMDA receptor subunits: function and pharmacology,” *Curr. Opin. Pharmacol.*, vol. 7, no. 1, pp. 39–47, 2007.

[68] J. T. R. Isaac, M. Ashby, and C. J. McBain, “The Role of the GluR2 Subunit in AMPA Receptor Function and Synaptic Plasticity,” *Neuron*, vol. 54, no. 6, pp. 859–871, 2007.

[69] D. Nutt, “GABA A Receptors: Subtypes , Regional Distribution , and Function,” *J. Clin. Sleep Med.*, vol. 2, no. 2, pp. S7–S11, 2006.

[70] F. Malerba, F. Paoletti, B. B. Ercole, S. Materazzi, R. Nassini, E. Coppi, R. Patacchini, S. Capsoni, D. Lamba, and A. Catteneo, “Functional Characterization of Human ProNGF and NGF Mutants : Identification of NGF P61SR100E as a ‘ Painless ’ Lead Investigational Candidate for Therapeutic Applications,” *PLoS One*, vol. 10, no. 0, pp. 1–34, 2015.